Design, modelling, characterization and implementation of acoustic lenses for modulation of ultrasound beams.

Ph.D.

November 2020

Author: Daniel Tarrazó Serrano

Advisors: Dr. Antonio Uris Martínez
           Dra. Constanza Rubio Michavila

Agraïments

En primer lloc, agrair a tots i totes aquells que m'heu ajudat durant aquest llarg viatge. Una part de la culpa d'aplegar fins ací la tenen Joan Escrivà Arlandis i Abel Soler Calatayud; canyeta, peixet i la cassalla a colpets. També agrair a la meua germana, la meua mare i el meu pare, per tot el seu afecte i suport (a més de la paciència infinita). Als meus directors, Antonio i Constanza pel seu temps i ajuda, no només en la part tècnica, sinó en la que transcendeix més enllà en l'escriptura d'una tesi. Gràcies Pilar Candelas per haver confiat en mi per complir amb els objectius de la investigació, sense ella no hauria pogut accedir a un contracte predoctoral. José Miguel Fuster, gràcies per estar en el grup i ha estat un plaer treballar amb tu al teu costat. De la mateixa manera, Sergio Castiñeira Ibáñez ha estat un company fonamental per arribar a aquest punt. Juan Carlos Melgarejo i la seua parella han donat un cop de mà amb la revisió de l'anglès a més de passar uns mesos compartint casa i vaixell. L'Holandès sempre ha de tenir un capità. Amb Sergio Pérez López he compartit hores de despatx, congressos i patiments diversos. A aquells i aquelles del Departament de Física Aplicada de la Universitat Politècnica de València que m'heu dipositat la vostra confiança. Especialment a Paco Belmar, director de el Centre de Tecnologies Físiques que ha estat el mestre de la gestió. Tampoc m'oblide d'aquells que m'han ajudat a mantindre el seny al llarg d'aquests anys. Perquè compartir el saxo i moments de comboi amb l'equip fusta, un trompeta que no pot torrar i un guitarrista polifacètic i les seues parelles, en el fons ha estat fonamental per no abandonar aquest projecte.

I per descomptat, a tu, la meua vida i el meu amor, Cuca Nácher.

Ars longa, vita brevis.

Abstract

The ability to control and modify energy beams has been the subject of research by the scientific community for a long time. In the acoustic field, this energetic control of mechanical waves has numerous applications. From industrial, food, pharmaceutical applications, et cetera, to biomedicine. This thesis is based on the ultrasound control and focal modulation applications. It is possible to modulate and control the ultrasound focii in different ways. In this case, flat lenses were developed based on the principle of diffraction to focus the beams. The advantages of using flat focusing lenses allow them to be easily implemented in machining and drilling processes and even through 3D printing. It was proposed to use planar transducers that when emitting on an acoustic lens, controlled characteristics of focal conformation were produced. The lens known as Fresnel Zone Plane (FZP) was chosen as the implementation design basis for the different solutions that manage to fulfill the objectives set.

By applying modifications to an FZP it was possible to go from a lens with extraordinary focusing capabilities to a lens that was capable to control lateral resolution, depth of focus and even improving the gain. The final objective application was the use in high intensity ultrasound transducers known as HIFU. Improving the ability to resolve makes it possible to develop better cancer therapies that represent a higher rate of success in the fight against cancer. In the present thesis, a novel FZP lens based on phase change has also been proposed that can be a before and after in biomedical applications. It has not only been possible to improve the efficiency of an FZP, but it has also been possible to implement it in materials compatible with magnetic resonance imaging.

Numerical models based on the finite element method were developed for emulating the involved physics. Measurements were carried out under controlled conditions by a high precision robotic system. All the results obtained and published were developed numerically and experimentally, validating the working method and giving consistency to the proposed solutions.

Resum

La capacitat de controlar i modificar els feixos d'energia ha sigut motiu d'investigació per part de la comunitat científica des de llarg temps arrere. En el camp de l'acústica, este control energètic de les ones mecàniques té nombroses aplicacions. Des de les aplicacions industrials, alimentàries, farmacèutiques, etcètera fins la biomedicina. Esta tesi es basa en l'aplicació del control i modulació focal dels ultrasons per a l'ús en este últim camp. Es pot modular i controlar els focus d'ultrasons de diferents formes. En este cas, s'han desenvolupat lents planes que utilitzen el principi de la difracció per a aconseguir focalitzar els feixos. Els avantatges de l'ús de lents planes de focalització permeten ser implementades de forma senzilla en processos de mecanització i inclús per mitjà d'impressió 3D. Es proposa utilitzar transductores plans que a l'emetre sobre una lent acústica, es produïsca una conformació focal de característiques controlades. La lent coneguda com a lent de Fresnel (FZP) ha sigut triada com a base de disseny en la implementació de les diferents solucions que aconseguixen complir amb els objectius marcats.

Per mitjà de l'aplicació de modificacions en una FZP es pot aconseguir passar d'una lent amb capacitats extraordinàries de focalització a una lent capaç de controlar la resolució lateral i la profunditat de focus i inclús millorar el guany. L'objectiu final d'aplicació és l'ús en transductores d'ultrasons d'alta intensitat coneguts com HIFU. Millorar la capacitat de resolució fa que es puguen desenvolupar millors teràpies oncològiques que suposen un índex major d'èxit en la lluita contra el càncer. En la present tesi s'ha proposat, a més, una nova lent FZP basada en el canvi de fase que pot resultar un abans i un després en aplicacions biomèdiques. S'ha aconseguit no sols millorar l'eficiència

d'una FZP, sinó que s'ha aconseguit implementar en materials compatibles amb ressonància magnètica.

S'han desenvolupat models numèrics basats en el mètode dels elements finits que emulen la física involucrada. Les mesures han sigut realitzades en condicions controlades per un sistema robotitzat d'alta precisió. Tots els resultats obtinguts i publicats han sigut desenvolupats de forma numèrica i experimental, validant-se el mètode de treball i donant consistència a les solucions proposades.

Resumen

La capacidad de controlar y modificar los haces de energía ha sido motivo de investigación por parte de la comunidad científica desde largo tiempo atrás. En el campo de la acústica, este control energético de las ondas mecánicas tiene numerosas aplicaciones. Desde las aplicaciones industriales, alimentarias, farmacéuticas, etcétera hasta la biomedicina. Esta tesis se basa en la aplicación del control y modulación focal de los ultrasonidos para el uso en este último campo. Se puede modular y controlar los focos de ultrasonidos de diferentes formas. En este caso, se han desarrollado lentes planas que utilizan el principio de la difracción para lograr focalizar los haces. Las ventajas del uso de lentes planas de focalización permiten ser implementadas de forma sencilla en procesos de mecanización e incluso mediante impresión 3D. Se propone utilizar transductores planos que al emitir sobre una lente acústica, se produzca una conformación focal de características controladas. La lente conocida como lente de Fresnel (FZP) ha sido escogida como base de diseño en la implementación de las diferentes soluciones que logran cumplir con los objetivos marcados.

Mediante la aplicación de modificaciones en una FZP se puede lograr pasar de una lente con capacidades extraordinarias de focalización a una lente capaz de controlar la resolución lateral y la profundidad de foco e incluso mejorar la ganancia. El objetivo final de aplicación es el uso en transductores de ultrasonidos de alta intensidad conocidos como HIFU. Mejorar la capacidad de resolución hace que se puedan desarrollar mejores terapias oncológicas que supongan un índice mayor de éxito en la lucha contra el cáncer. En la presente tesis se ha propuesto, además, una novedosa lente FZP basada en el cambio de fase que puede resultar un antes y un después en aplicaciones biomédicas.

Se ha conseguido no solo mejorar la eficiencia de una FZP, sino que se ha conseguido implementar en materiales compatibles con resonancia magnética.

Se han desarrollado modelos numéricos basados en el método de los elementos finitos que emulan la física involucrada. Las medidas han sido realizadas en condiciones controladas por un sistema robotizado de alta precisión. Todos los resultados obtenidos y publicados han sido desarrollados de forma numérica y experimental, validándose el método de trabajo y dando consistencia a las soluciones propuestas.

Contents

List of Figures

List of Tables

Chapter 1

Background and objectives

1.1 Background Introduction

Biomedical research has aroused interest in recent years in the scientific community. Engineering and medical science union has been a before and after in the history of medicine. One of the most common diseases with a relatively high mortality rate in advanced societies of this century is cancer. This thesis began in 2016. This project was presented to the Ministry of Economy and Competitiveness with the figures associated to the Spanish Society of Medical Oncology (known by its acronym in Spanish as SEOM) report at that moment. That figures estimated an incidence of 210,000 new cancer cases per year in the Spanish population (Cruz 2013). Current SEOM report estimates that cancer continues to be one of the main causes of morbidity and mortality and that diagnosed cases will reach slightly more than 277,000 (REDECAN 2020). The most common cancers diagnosed in Spain are breast cancer, followed by colon and rectum, lung, prostate and urinary bladder cancers (Figure 1.1). Therefore, cancer continues being a disease that causes millions of deaths in the world. The morbidity and mortality 2018 record rate in the world was 18.1 million (WHO 2020a; IARC 2020). It is reckoned that in the next 20 years the incidence will increase to 29.5 million (WHO 2020b). Studies have shown that cancer causes about half of deaths in middle-aged people (Karim-Kos et al.

2008). These data justify that public research should invest resources in the development of diagnostic and treatment systems of such desease.
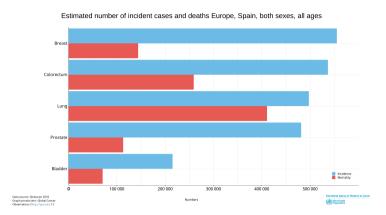
Figure 1.1: Cancers with the highest prevalence comparison between the number of cases and deaths in Spain.

It is known that a crucial factor to overcome the disease is an early diagnosis. Development of tools that have better sensitivity and detection capabilities contribute to achieve this goal. Cancer currently has multiple forms of treatment. Some treatments are more invasive than others (Doroshow 2016; Doroshow 2016; Institute 2019). Over the years, treatments have been developed for being more effective and more efficient as well as less patient invasive and harmful (Fetting et al. 1996). Surgery is the most common invasive treatment for various types of cancer. This system is based on the surgical removal of the tumor. Other treatments that do not involve admission into an operating room are chemotherapy, radiation therapy and targeted therapy. These procedures also cause collateral damage to the patient.

Chemotherapy uses drugs that attack and destroy tumor cells. It can be an intravenously or orally treatment. One of the cons of using these treatments is the indirect damage caused on the patient. Additionally, cancer cells that survive to a treatment develop immunity. This immunity is replicated in the new cells. Treatment known as radiation therapy is often combined with chemotherapy. Radiation affects much more to those cells with higher activity. Cancer cells have a higher growth rate and energy consumption than a healthy cell. Therefore, they absorb more radiation and this prevents their division and growth. More current treatments such as targeted therapy are based on chemotherapy. The difference is found in adding to the drug a molecule (an-

tibody, enzyme, etc.) that manages to detect and attack only cancer cells. Another type of process is hormonal therapy. Hormones are used to slow growth in cancers that affect the reproductive system or breasts. Some current therapies such as laser therapy, photodynamics or cryotherapy cause less secondary damage to the patient. Laser therapy uses the precision and resolution of the beam light to seal lymphatic vessels, burn body outside tumors or inside tumors through catheters, etc. This treatment is combined with other treatments such as those mentioned above. Photodynamic therapy bases its operation on introducing drugs with light reaction molecules. Using laser or infrared, the drug attached to tumor cells reacts killing these cells. This thesis is based on the devices development that help with treatments based on temperature change. In this case, it is not about cryotherapy, which is based on sufficiently cooling cancer cells, but about hyperthermia treatments. Hyperthermia is a treatment that destroys a cancer cell by adding heat to it. One of the advantages of this treatment is that it can be used to treat any part of the body either any size. Hyperthermia treatment can be performed using a device that is inserted into the body or from outside the body. One of the most widespread hyperthermia treatment systems with the highest clinical experience is the High Intensity Focused Ultrasound known as HIFU (Kennedy 2005).

Ultrasounds are mechanical waves that dissipate their energy in heat energy when they pass through a medium. Energy dissipation can raise the temperature enough to cause damage to the cell wall and therefore destroy the cancer cell when several ultrasound beams are focused on a specific area. Temperature increasing can be due to two factors, the dissipated energy accumulation or cavitation phenomenon. It is important to obtain a controlled coagulative necrosis. For this purpose, it is necessary to have a temperature between 60° C and 100° C. It is dangerous to overcome 100° C due to it would bring the tissue to the boiling point (Kennedy, Ter Haar, and Cranston 2003). The capacity with which the temperature is able to increase in the tissue depends on multiple factors: the shape of the tissue, the absorption coefficient and the exposure duration. Neither the shape nor the absorption coefficient of the tissue can be modified. Therefore, this work has focused on duration of exposure controlling. The fundamental idea is achieving the temperature increase in the affected area in the most precise way possible and in the shortest time. If the treatment lasts for a long time, the heat can dissipate to the adjacent areas to the treatment area, affecting healthy cells.

There are several advantages using HIFU proceeding. This treatment involves less risk to the patient. The time reduction in hospitalization reduces the noso-

cominal infections risk (Wenzel 1995). In addition, this technique can be used in older patients or with other health problems due to the technique does not have secondary damages that could affect the rest of the body. This procedure has a wide margin for improvement, as has been seen in recent years and throughout the development of this doctoral thesis. Current commercial systems serving HIFU treatments use ultrasonic transducers with concave-convex geometric shapes. Some of them are attached to probes that are introduced rectally, for example, to treat prostate cancer using HIFU. The hypothesis is to develop passive systems that focus the ultrasound beams with flat transducers. The fact of having a passive targeting system in a planar transducer means that a single HIFU transducer can be used for several treatment objectives.

There is the half wavelength spatial resolution limitation if concave-convex transducers are used. To achieve higher resolutions, as could be seen the case of optics (Zhu et al. 2011), the use of subwavelength structures is required. The objectives set out in this thesis involve the use of this type of structures for ultrasound focusing. Subwavelength are structures that modulate acoustic beams through structures smaller than the wavelength. These structures base their modulation capacity on diffractive effects. Gain and resolution improvements can be obtained by creating different geometric paths, enhancing constructive interferences and blocking destructive ones. In this way, they can achieve high resolutions that allow getting smaller targets and improving precision. Gain enhancement reduces the input power of the HIFU. By reducing the power it is possible to cause less damage to adjacent tissues, a shorter treatment duration, etc.

Flat structures that can occupy the least possible space and that are also easy to mechanize and implement are very interesting. In this way, these structures can be used by coupling them directly to the transducer. The devices that have been developed in this thesis do not rely heavily on resonances. Other studied subwavelength structures are highly dependent on Fabry-Perot resonances, Lamb modes, and periodicity (Estrada et al. 2008; Estrada et al. 2009; Gomez-Lozano et al. 2014). In this case, the use of Fresnel lenses (FZP) provides an extraordinary transmission that meets the objetive requirements (Molerón, Serra-Garcia, and Daraio 2014). FZPs are binary structures that are distributed to focus achieving at a given focal point for a given wavelength. More detail on these structures will be found in subsequent chapters (chapter 3, chapter 4, chapter 5, chapter 6, chapter 7).

1.2 Objectives

The objectives of this doctoral thesis are based on those projects included in the TEC2015-70939-R project (MINECO / FEDER). Before listing the objectives, it must be considered which characteristics are relevant and where improvements can be made in a HIFU based treatment. On one hand, it might be possible to make changes to the piezoelectric design by completely modifying the transducer. On the other hand, using the same transducer, it is possible to introduce passive elements that achieve the same objective without having to use different transducers for each objective. This thesis objectives are aimed at the development of passive elements that are able to modulate the ultrasound beams to achieve this purpose. Therefore, they have been divided into general and specific objectives. Two general objectives were determined with one sub-objective each and three specific objectives.

<div align="center">General Objectives</div>

1. Increasing resolution capacity in tumor ablation with HIFU transducers.

   1.1 Study and design of new HIFU transducers using subwavelength structures based acoustic lenses to achieve the configuration of the focal zone (control of the ablation volume improvement).

2. Decreasing patient exposure time to HIFU therapy.

   2.1 Study and design of extraordinary transmission subwavelength structures that increase focal gain in 3 dimensions.

<div align="center">**Specific Objectives**</div>

1. Thoroughly study the main characteristic parameters of HIFU transducers.

2. Developing and analyzing models based on proposed acoustic lenses using Finite Element Method (FEM) that describe the sound beams propagation considering the physics involved.

3. Numerical results experimental validation.

1.3   Document structure

Chiefly, I want to acknowledge the following public funding sources that have made possible this research.

In this thesis, five scientific articles have been included. The first three articles are interrelated and were realized in collaboration with researchers from Tomsk Polytechnic University. It was used a concept so-called reference radius/phase in FZP lenses. The study of its influence on acoustic lenses had never been done before. It was discovered that the introduction in the lenses construction of this parameter could be interesting in the ultrasonic beam modulation. Due to the apodization effect, explained in more detail in the articles, the spatial resolution of an FZP lens can be controlled. In the last two articles, materials that were Magnetic Resonance Imaging (MRI) compatible and could be used in medicine were studied. In addition, the use of these materials had to equal or improve acoustic parameters compared to the materials that were being used to implement Soret-type lenses such as brass. The idea of a phase reversal lens succeeded in improving the efficiency of a Soret FZP type lens by more than 200%. The last article explains in detail the concept of the Phase-Reversal FZP (PR-FZP). All the data of the articles included in this thesis have been exposed as established by the regulations of the Doctoral School of the Universitat Politècnica de València. These data includes titles, all the authors, journal, year of publication, volume, page or article number, impact factor and their rank based on the Journal Citation Index.

Title: "Manipulation of focal patterns in acoustic Soret type zone plate lens by using reference radius/phase effect"
Authors: Tarrazó-Serrano, D., Rubio, C., Minin, O. V., Candelas, P., & Minin, I. V.
Journal: Ultrasonics
Year: 2019
Volume: 91
Pages: 237-241

Impact Factor: 3.065
Rank (Acoustics): 6/32 (Q1,T1), JIF 82.813

Title: "Design of Acoustical Bessel-Like Beam Formation by a Pupil Masked Soret Zone Plate Lens" **(Open-Access)**
Authors: Tarrazó-Serrano, D., Castiñeira-Ibáñez, S., Minin, O. V., Candelas, P., Rubio, C., & Minin, I. V.
Journal: Sensors
Year: 2019
Volume: 19(2)
Article number: 378
Impact Factor: 3.275
Rank (Instruments & Instrumentation): 15/64 (Q1/T1), JIF 77.344

Title: "Tunable depth of focus of acoustical pupil masked Soret Zone Plate"
Authors: Castiñeira-Ibáñez, S., Tarrazó-Serrano, D., Minin, O. V., Rubio, C., & Minin, I. V.
Journal: Sensors and Actuators A: Physical
Year: 2019
Volume: 286
Pages: 183-187
Impact Factor: 2.904
Rank (Instruments & Instrumentation): 19/64 (Q2/T1), JIF 71.094

Title: "MRI Compatible Planar Material Acoustic Lenses" **(Open-Access)**
Authors: Tarrazó-Serrano, D., Castiñeira-Ibáñez, S., Sánchez-Aparisi, E., Uris, A., & Rubio, C.
Journal: Applied Sciences
Volume: 8(12)
Article number: 2634
Notes: This article belongs to the Special Issue Modelling, Simulation and Data Analysis in Acoustical Problems. Impact Factor: 2.474 Rank (Engineering, Multidisciplinary): 32/91 (Q2), JIF 65.385
Rank (Applied Physics): 62/154 (Q2), JIF 60.065

Title: "Acoustic Focusing Enhancement in Fresnel Zone Plate Lenses" **(Open-Access)**
Authors: Tarrazó-Serrano, D., Pérez-López, S., Candelas, P., Uris, A., & Rubio, C.
Journal: Scientific Reports
Year: 2019
Volume: 9(1)

Pages: 1-10
Impact Factor: 3.998
Rank (Multidisciplinary Sciences): 17/71 (Q1,T1), JIF 76.761

Chapter 2

Experimental Measurements

Due to the characteristics of the acoustic experiments that are carried out in an immersion situation, it was necessary to develop a completely automated data acquisition system that allows the attainment of pressure data at any point in the space of the immersion tank. Through these results, it is possible to characterize the behavior of the different acoustic devices developed by the group. The name of the complete acquisition system is Archimedes. Archimides system allows the movement and acquisition of acoustic parameters in the three spatial dimensions as well as its remote control in an automated way. Archimedes can be divided into 3 fundamental parts: the robotic system with its motion control, the data acquisition system, and the transducers and amplifiers that are used for the generation, transmission and reception of ultrasonic waves.

The robot was built based on the size of the immersion tank where the tests are carried out, which contains distilled water (demineralized and deionized) and is 0.5 meter wide by 0.5 meter high by 1 meter long. These dimensions assume that the immersion tank must contain around 200 liters of distilled water to be functional and to allow both the transducers and the devices to be completely submerged, and to avoid reflections due to changes in impedance caused by a medium change.

The parts that make up the robot (Figure 2.1) are: the holding structure or frame, three Cartesian arms, the sampling arm and the manual sensor arm. Archimedes allows to control the Cartesian and sample arms. The sampling arm also has a servo motor to rotate the transducer (in azimut). The Cartesian arms allow for the control and automation of the positioning in the 3 spatial dimensions (x, y, z). Each of the arms oversees the movement in one of the three axes. The sampling arm, despite having the rotation servo motor, allows manual adjustment along the x and z axes to be able to place the sample at the desired distance and height. Finally, the transducer arm of the sensor is completely manual. This allows the position of emitting transducer to be adjusted in any tank position, although without the freedom to change its position during measurements.
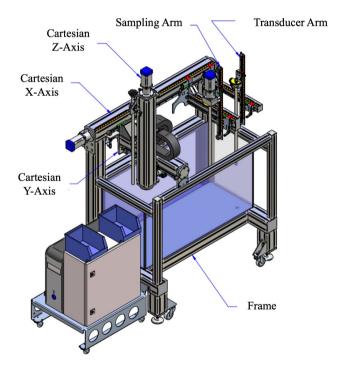
Figure 2.1: Archimedes structure scheme. The robot is mounted on the immersion tank.

The operation of the robot is as follows: each one of the servomotors is connected to a controller that regulates the current supply to them and regulates the movement pace. The minimum step the sampling arm is able move in each of the axes is 0.005 mm. In the case of the servomotor that controls

the azimuth, the spatial resolution can be transferred to an angular resolution of 0.144^o. The controllers are in turn connected to a model board PCI-7330, from National Instruments, which is responsible for directing the robot's movements. The movement of the arms with servo motors is controlled by Archimedes control software. This program allows the design and automation of the experimental measurements, since planes or measurement volumes can be established configuring the movement of each of the positioning axes. As safety measures added to the mechanical system, there are limit switches that prevent one arm from colliding with another and avoid any damage caused by a programming error. Additionally, there is an emergency stop button that immediately stops the movement of the robot. Once the robot is turned on and the 3DReAMSUltra control program starts, a system self-calibration is performed. This calibration is based on placing the Cartesian arm at the coordinate origin and leaving the sample arm at an azimuth of 0°.

Finally, it should be noted that the robot is built in accordance with the directives and regulations that govern industrial safety. The directives 2006/42/CE on machinery; the directive 73/23/CEE modified by the 2006/95/CEE of low tension, the directive of electromagnetic compatibility 92/31/CEE modified by the 93/68/CEE and 2004/108/CE. In addition to the harmonized standards UNE-EN 1050, UNE-EN 418, UNE-EN 954 and UNE-EN 60204-1 that regulate the safety of machinery, risk assessment, emergency stops, design and electrical equipment respectively.

The data acquisition system consists of the NI PCI-7330 motion control card, the PicoScope 3224 digital oscilloscope and the Archimedes control software for data acquisition, developed at LabVIEW. The NI PCI-7330 card controls the robot as its dual processor architecture processes up to four axes of coordinated movement in real time. This card calculates the instantaneous position and controls the acceleration and speed of the axis movement to the marked position. A PicoScope 3224 digital oscilloscope connected to the computer via USB is used to obtain the signals. The oscilloscope has two channels and takes samples with a resolution of 12 bits. It has a dynamic range of 72 dB and a bandwidth of 10 MHz. Both the control board and the oscilloscope are controlled by the Archimedes control software installed on the acoustic laboratory computer.

One of the most important elements for the measurement of acoustic planes is the hydrophone. The CTF features a Precision Acoustics hydrophone, model 1.0mm Needle Hydrophone (Figure 2). This hydrophone is capable of measuring high frequencies, even if their signal level is very weak. The hydrophone sensitivity is 850 nV / Pa (-241.4 dB @ 1V / uPa) with a tolerance of +/- 3

dB. The frequency response is flat $+/-$ 2 dB between 3 and 12 MHz and $+/-$ 4 dB between 200 kHz up to 15 MHz. The bandwidth ranges from 5 kHz up to 15 MHz. Figure 2.2 shows the experimental set-up and different acoustic devices measured during the research.
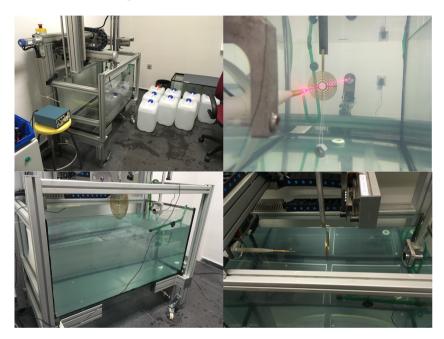
Figure 2.2: Archimedes measurement system and different experimental set-ups.

Chapter 3

Manipulation of focal patterns in acoustic Soret type zone plate lens by using reference radius/phase effect

3.1   Abstract

The manipulation of focal patterns of acoustic underwater Soret Zone Plate lens in far fields, such as manipulation (optimization) of Sidelobe Level and the design of long depth of focus by selecting the simple free parameter called reference radius (phase) has been demonstrated.Two effects have been studied by means of numerical simulations. Regarding the first effect, simulations

demonstrate diffraction limited focal spot (0.47 wavelength) and 3 dB reduction of the first Side Lobe Level using Soret ZP with an optimal reference radius and without causing neither main lobe broadening or gain reduction. In the second effect, by using numerical simulations an increasing of depth of focus, more than 2 times, in comparison with classical Soret ZP with high numerical aperture (F/D = 2.5), was observed.

3.2 Introduction

A lens is a device that can manipulate waves by taking advantage of both their refractive and diffractive properties to produce wave focalization. Acoustic lenses have attracted the attention of scientists around the world for their application in multiple areas of industry, engineering, acoustic tweezers, biomedicine and for other applications requiring low-cost acoustic focusing lenses (Vilkhu et al. 2008; Albu et al. 2004; Li et al. 2003; Illing et al. 2005; McCann and Forde 2001; Calvo et al. 2015b; Amemiya et al. 1997; Hon et al. 2010; Tu, Chen, and Hwang 2016; Schonbrun, Rinzler, and Crozier 2008), to mention a few. This explains why their design is subject of much research nowadays. One of the effects of these lenses is their capability of focalization, which it can be obtained by means of different types of methods and techniques.

Acoustic lenses based on phononic crystals have been designed and fabricated (Cervera et al. 2001). Other types of acoustic lenses are those designed with a refractive index that varies throughout the medium continuously. These are the so-called Gradient-Index (GRIN) lens, and the variation of the refractive index is achieved by forming labyrinthine structures (Li et al. 2012; Welter et al. 2011; Peng, Xiao, and Wu 2014). Acoustic metamaterials (Guenneau et al. 2007) and acoustic resonators Molerón, Serra-Garcia, and Daraio 2014) have also been used in the design of acoustic lenses.

There are also acoustic devices that focus sound through the phenomenon of diffraction. Acoustic lenses based on constructive interferences of diffracted fields, such as Fractal Lenses or Fresnel Zone Plates (FZP), are a good alternative to refractive lenses. FZP lenses have advantages in situations where size, weight, system complexity and fabrication are important O'Shea et al. 2004; Zhang, Yin, and Fang 2009). The classic FZPs that are implemented alternating transparent to opaque Fresnel zones are called Soret Zone Plates (SZP) (Soret 1875). This work is focused on this type of Fresnel's lenses.

In Clement, Nomura, and Kamakura 2015 the authors study a lens formed by slits of different thickness located at r_n, while in the present work rigid scat-

tered located at r_n (r_n a radius of n-th Fresnel zone) has been used. Following Babinet's principle considerations, both approaches can be considered equivalent. Recently Calvo et al. (Calvo et al. 2015a) fabricated and characterized an underwater acoustic SZP lens with alternating transparent and opaque zones made of soft silicone rubber. Calculations shown some reduction of the first Side Lobe Level (SLL), but with a main lobe broadening.

Although the diffraction of the acoustic field produce a maximum pressure field in the axis, the focal point shows some miss-definition due to the existence of secondary lobes Bashford et al. 1997; Kanevsky 1977; Shimizu, Chubachi, and Kushibiki 1989). In such a way, the relationship between the main and secondary lobe, known as SLL, is one of the main problems that SZPs can exhibit (Minin and Minin 2008).

Even though the maximum energy is obtained at the Focal Length (F_L), the SLL are not high enough with SZP lenses for applications where high precision is required. In this regard, a new technique used in biomedicine such as High Intensity Focused Ultrasound (Aubry et al. 2013; Escoffre and Bouakaz 2015), both in acoustical printer (Amemiya et al. 1997) or in acoustical particle manipulations (Tu, Chen, and Hwang 2016) requires very precise targeting area so it is desirable to be able to control the lobes of the transmitted signal.

In other fields of physics, such as electromagnetism, this problem has already been raised. Igor V. and Oleg V. Minin (Minin and Minin 1990) studied the possibility of altering the energy distribution function in a predetermined focus area. Recently, the authors themselves have shown that by choosing a radius of the first zone or a reference phase, non-standard values of the SZP radii can be obtained which improve the performance of the antennas and add a new application to the antennas zone plates (Minin and Minin 2011b) add and in communications to preferentially suppress the clutter return relative to the desired main beam signal (Webb, Minin, and Minin 2007).

The present study investigates numerically an alternative SZP design to reduce or manipulate the lobes of the transmitted acoustic signal for an underwater SZP. A $\lambda/6$, where λ is the wavelength, thin SZP and 15 Fresnel zones width is thereby obtained in simulation showing different phenomena such as side lobe corrections and ultra-wide beam pattern. The simulations have been carried out using the Finite Element Method (FEM) (Chan et al. 1995; Zienkiewicz et al. 1977).

3.3   Theorical analysis and simulation

A SZP is structured in concentric circular sections known as Fresnel Regions. Each Fresnel Region has the same surface and makes the same contribution to the focusing procedure. Consecutive Fresnel Regions have a 180° phase shift between them and they interfere destructively. Among other, the main SZP design parameters to deal with are F_L that is the location, in the axial coordinate, where the acoustic pressure field is focused; the Number of Fresnel Zones (N) which include both opaque and transparent circular sections; the Design Frequency (f), it is the frequency at which the lens is expected to focus at the (see Figure 3.1a). Once the design values have been set, the radial distances of the implemented lens can be obtained using the Equation (3.1) which depends on all the previous design parameters and is valid for plane wave incidence.

$$r_n = \sqrt{n\lambda F_L + \left(\frac{n\lambda}{2}\right)^2} \tag{3.1}$$

On the other hand, in the earliest work was recognized the existence of a free parameter in the design of zone plates,where the radius of the central Fresnel zone were treated. This radius is known as the reference radius (Minin and Minin 1990) and it is the new free parameter. It should be noted that the choice of the first zone as the reference is arbitrary. From the point of view of geometrical optics, the introduction of a reference radius does not change the properties of the zone plate. However, in the wave approximation this is not so. This reference radius is equal to introducing a variable reference phase (Minin and Minin 2011b).

In other words, another parameter that can be varied in calculating the modulation function of a zone plate is a permanent phase shift. The quasi-Fresnel radii can be displaced by adding an initial phase shift to the phase function of the SZP. This means in fact that the zone is divided not by starting at the extremum of the transmission phase function but at an arbitrary value of transmission (Minin and Minin 2011b). In this case for binary zone plate the quasi-Fresnel radii will be defined by the Equation (3.2) (Minin and Minin 2011b):

$$r_n = \sqrt{n\lambda\sqrt{F_L^2 + r_0^2} + \left(\frac{n\lambda}{2}\right)^2 + r_0^2} \tag{3.2}$$
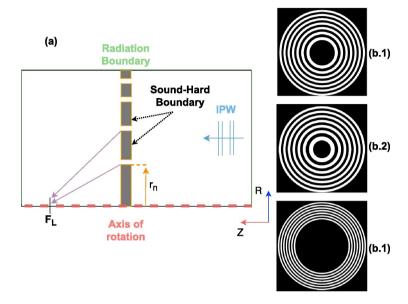
Figure 3.1: (a) FEM Scheme. In blue, the boundary of the Incident Pressure Wave (IPW), in green radiation condition boundaries and in red axis of rotation. SZP zones are considered rigid. (b.1) SZP with $r_0 = 0$, (b.2) Amplitude mask of SZP with $r_0 \ll r_1$, (b.3) Amplitude mask of SZP with $r_0 \gg r_1$. Note that for visual information the picture (b.2) is not in scale.(For interpretation of the references to colour in this figure legend, the reader is referred to the web version of this article.)

In order to study the physical phenomena involved in the interaction between the ultrasound waves and the lenses, it has been necessary to implement a mathematical model that replicates the characteristics of the system. Commercial FEM software COMSOL Multyphysics (Multiphysics 2012) has been used to determine the distribution of acoustic pressure and how the generated sources remain once the waves interact with the lens and diffract, causing the interference phenomena. FEM provides an approximate numerical solution of the model. This method performs a discretization of the model and solves the Helmholtz Partial Differential Equation (PDE) described in the equation Equation (3.3).

$$\nabla \left(-\frac{1}{\rho} \nabla p \right) = \frac{\omega^2}{\rho c^2} p \tag{3.3}$$

All the SZP lenses (including or not radius/phase reference) are axisymmetric, the model has been simplified by implementing a half-lens and applying a rotation with its central axis as the center for its complete generation. This facilitates the reduction of the degrees of freedom necessary to obtain the results of the numerical simulation and thus reducing the calculation time and its complexity. In this work, underwater acoustic transmission is considered. To solve the Helmholtz equation Equation (3.3), typical values of water such as density of the medium ($\rho = 1000$ kg/m^3) and sound propagation velocity ($c = 1500$ m/s) have been taken. The working frequency (f) of both lenses was 250 kHz. Therefore the wavelength (λ) was 6 mm. It can be found at Equation (3.3) by its relationship with the angular velocity (ω). Finally, p corresponds to the acoustic pressure. The initial conditions of the model were the following: Initial pressure (p_0) was zero and the thickness of the lenses was 1 mm which was despicable with respect to the wavelength of the incident pressure wave. The defined boundary conditions were: the lenses were considered infinitely rigid marking the contours of the elements applying the Newmann condition (the sound velocity in the contour was zero); the contours of the model were defined as wave radiation condition boundary to emulate an infinitely large medium and therefore the Sommerfeld condition was satisfied; the axis of rotation was defined as axis of axisymmetry to simulate the 360° rotation that makes up the SZPs in 3D. The geometry of the mesh used was triangular. A maximum element size of $\lambda/8$ and a minimum of $\lambda/14$ was established to avoid numerical dispersion in the simulations. In Figure 3.1 the scheme of the model implemented in FEM is shown.

3.4   Results

The Numerical Aperture (NA) of the lens design must be taken into account. NA is defined as F_L divided by the diameter of the lens (D). It is well known that the Rayleigh resolution is determined by the numerical aperture of the lens and the wavelength of the radiation used. The smaller the NA, the better is the resolution of the lens. Taking into account that it must be designed with a small numerical aperture, a value NA of 0.214 has been selected for simulation. By selecting a focus position at 27 mm in axis of symmetry, a maximum lens diameter of 126 mm is obtained that complies with the chosen NA.

Therefore, the design of the SZP will comply with these characteristics implemented in the construction equation Equation (3.1), taking into account that λ was 6 mm for the case of the host medium is water. To design the SZP

with radius/phase reference, two cases are considered. Given the construction equation Equation (3.2), a reference radius must be chosen for each case. The first one, is that r_0 is smaller than the first radius (r_1) of the original SZP ($r_0 \ll r_1$). The second case occurs when r_0 is bigger than r_1 ($r_0 \gg r_1$).

The results are expressed as a function of the Intensity Level (IL), that is defined as the ratio, in dB, between the downstream intensity (I) and the incident intensity (I_{inc}).

$$IL = 10 \log \left(\frac{I}{I_{inc}} \right) \tag{3.4}$$

SLL reduction

In the first case, a reference radius smaller than the first radius of a classical SZP has been taken. The numerical results are shown below. In Figure 3.2a longitudinal section is shown for the optimal case compared with the original SZP. It can be seen the position of the F_L has not been modified regardless of the r_0 chosen. In Figure 3.3 a cross section at the F_L position is made, in other words a cut in R axis is made. In this case, it can be seen that there is a modulation of the secondary lobes. An SLL increase of approximately 3 dB is produced. By the conservation energy law, a displacement of this energy is caused towards other lobes. Further, the energy in F_L is conserved. It is also followed from Figure 3.3 that FWHM for both cases is almost the same and equal to 0.47λ, which is near the diffraction limit.

In Table 3.1, a comparison is shown for different cases that meet the condition $r_0 \ll r_1$. As r_0 decreases, SLL increases until a limit value is obtained. Therefore, $r_0 = r_1/10$ has been selected as the optimum value since the SLL cannot be improved for selected values of NA.

Focus expansion

In the second case, values are taken above the first radius of the classical SZP. A longitudinal cut has been made in the same way as in the previous case that corresponds to the Z axis. It can be seen that despite maintaining the position of the maximum energy in the F_L, as r_0 increases, an energy expansion in the longitudinal axis is caused. In Figure 3.4, several higher reference radii than r_1 can be observed.
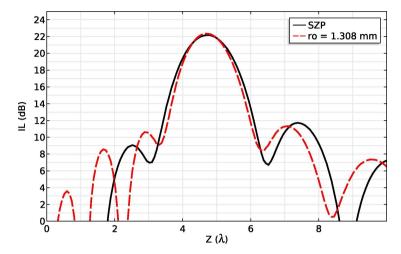
Figure 3.2: Numerical results of the Intensity Level (in dB) along Z axis. Comparison between classical SZP and SZP with reference radius r_0 ($r_0 = 1.308mm$) being $r_0 \ll r_1$. The results are shown for $f = 250$ kHz.

It could be noted that by selecting the reference radius, it may be controlled not only the first sidelobes (Figure 3.3) but also the main beamwidth to form ultra wide main beam. In Table 3.2, the value of the FLHM along the Z axis and the focal shift have been shown.The focal shift in SZP is completely dependent on the Fresnel number (N_F), which is determined by (Li and Wolf 1981).

$$N_F = \frac{D^2}{4\lambda F_L} \tag{3.5}$$

As it can be seen from Figure 3.1 and formula Equation (3.5), increasing the effective lens size (D), or reducing the focal length (F_L) or decreasing the working wavelength will increase the Fresnel number Equation (3.5), and thus, reduce the focal shift. Also in our design of SZP the focal shift increases with reference radius increasing. This effect was not previously observed.

For a reference radius of $r_0 = 50.20$ mm, the intensity referred to the incident intensity (I/I_{inc}) at the focus and at two points of half intensity drop (FLHM) along Z axis is shown in Figure 3.5. The inset of the figure shows an I/I_{inc} map. White discontinuous line point out the R axis cut which corresponds to FLHM points.
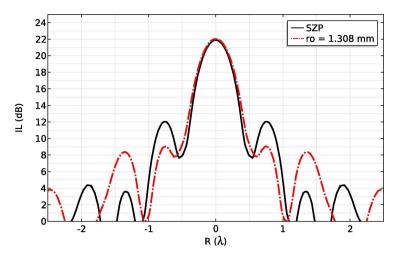
Figure 3.3: Numerical results of the Intensity Level (in dB) along R axis. Comparison between classical SZP and SZP with reference radius r_0 ($r_0 = 1.308mm$) being $r_0 \ll r_1$. The results are shown at the Focal Length (F_L) for $f = 250$ kHz.

3.5 Discussion and conclusions

A numerical study of the characteristics of the acoustic SZP with radius/phase reference has been carried out. Two cases have been studied in which two different phenomena are caused. As expected, a SLL reduction has been achieved when r_0 is minor than r_1. This is due to the control of constructive interference of diffracted waves from circular zones array. By changing the reference radius, the spatial frequency of the Fresnel zones has been changed. Having control over spatial frequency means being able to obtain a much finer focus, which in the case of applications such as HIFU, is of great interest as it allows to obtain a more precise foci.

In the case of being r_0 bigger than r_1, an expansion of the focus along the longitudinal axis is caused. This is due to 2 effects: one is the same as in the first case and the second one is amplitude apodisation effect. The latest is due to geometrical effect interpretation of central apodisation (obturation) on background sound, as the focus at the first diffraction order is in the shadow of the obturation for all other diffraction orders. Acoustic wave from negative orders is divergent and acoustic wave from positive orders above one, is rejected far from the center of the SZP (Vanderbei, Spergel, and Kasdin 2003). That

Table 3.1: Numerical values of Side Lobe Level (SLL) and Full Width Half Maximum (FWHM) for different values of the reference radius. Note that $r_0 = 0$ corresponds to SZP and the FWHM is obtained along R axis.

r_0 (mm)	SLL (dB)	FWHM (λ)
0	9.9	0.46±0.12
6.540($r_1/2$)	11.8	0.47±0.12
4.359($r_1/3$)	12.4	0.47±0.12
2.615($r_1/5$)	12.8	0.48±0.12
1.308($r_1/10$)	13.0	0.48±0.12
0.654($r_1/20$)	13.0	0.48±0.12
0.436($r_1/30$)	13.0	0.48±0.12

Table 3.2: Numerical values of Full Length Half Maximum (FLHM), Focus Shift and maximum Intensity referred to incident Intensity (I_{max}/I_{inc}) for different values of the reference radius along Z axis. Numerical value obtained for SZP designed F_L corresponds to 4.65λ.

$r_0(mm)$	FLHM(λ)	Focus Shift (λ)	I_{max}/I_{inc}
0	1.53	0	170
36.00 (r_6)	2.56	+0.30	118
50.20 (r_{10})	3.48	+0.55	86
60.23 (r_{13})	4.16	+1.05	73

is, a small fraction of the first order radiation is shifted to the higher order lobes.

To the best of our knowledge, the two designed and characterized focusing properties in this work, regarding the reference radius had been never studied previously in acoustics SZP lenses, making this work a great contribution to the field. Having these tunable properties will allow Fresnel lenses to be improved and further research to be made, given their possible applications in situations where better precision is required. For instance, the prospect of these results are important in some medical applications, where depending on the tumor or target area it is desirable either to have a finer focus, or an expansion of the focus.
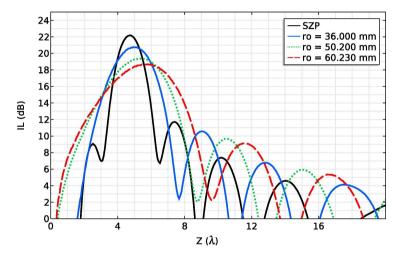
Figure 3.4: Numerical results of the Intensity Level (in dB) along Z axis. Comparison between classical SZP and SZP with reference radius r_0 that accomplish $r_0 \gg r_1$ for $f = 250$ kHz.
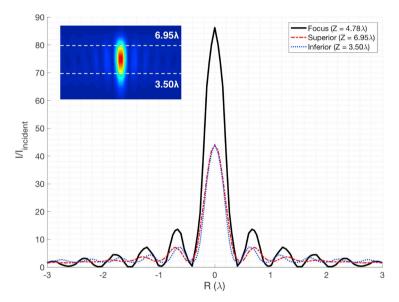
Figure 3.5: Intensity the intensity referred to the incident intensity (I/I_{inc}) at the focus (Z=4.78λ) and two points of half intensity (FLHM). Red dashed line corresponds to Z=6.95λ and blue dotted line to Z=3.50λ. The inset shows an I/I_{inc} map and the cut lines of FLHM for a SZP with a reference radius of $r_0 = 50.20$ mm. (For interpretation of the references to colour in this figure legend, the reader is referred to the web version of this article.)

Chapter 4

Design of Acoustical Bessel-Like Beam Formation by a Pupil Masked Soret Zone Plate Lens

Authors: Tarrazó-Serrano, D., Castiñeira-Ibáñez, S., Minin, O. V., Candelas, P., Rubio, C., & Minin, I. V.

4.1 Abstract

The image performance of acoustic and ultrasound sensors depends on several fundamental parameters such as depth of focus or lateral resolution. There are currently two different types of acoustic diffractive lenses: those that form a diffraction-limited spot with a shallow depth of focus (zone plates) and lenses that form an extended focus (quasi-Bessel beams). In this paper, we investigate a pupil-masked Soret zone plate, which allows the tunability of a normalized angular spectrum. It is shown that the depth of focus and the lateral resolution

can be modified, without changing the lens structure, by choosing the size of the pupil mask. This effect is based on the transformation of spherically-converging waves into quasi-conical waves, due to the apodization of the central part of the zone plate. The theoretical analysis is verified with both numerical simulations and experimental measurements. A Soret zone plate immersed in water with D/2F = 2.5 and F = 4.5λ changes its depth of focus from 2.84λ to 5.9λ and the lateral resolution increases from 0.81λ to 0.64λ at a frequency of 250 kHz, by modifying the pupil mask dimensions of the Soret zone plate.

4.2 Introduction

The necessity of manipulating waves has been one of the main objectives of the scientific community. Lenses are devices that achieve, through different physical phenomena such as refraction or diffraction, beam focusing and modulating effects. In the acoustic field, lenses have been developed for different areas such as biomedicine, engineering, and industry. One of the reasons why lenses are used in different fields is to reduce costs, since the use of lenses prevents the manufacture of new transducers (Pignoli et al. 1986; Amemiya et al. 1997; McCann and Forde 2001; Li et al. 2003; Albu et al. 2004; Illing et al. 2005; Vilkhu et al. 2008; Schonbrun, Rinzler, and Crozier 2008; Hon et al. 2010; Calvo et al. 2015b; Tu, Chen, and Hwang 2016). Due to the interest that these lenses have gained, their design and improvement is currently a research subject. One type of acoustic lens changes the refractive index between media, known as gradient-index lenses, using labyrinthine structures (Welter et al. 2011; Li et al. 2012; Peng, Xiao, and Wu 2014). Phononic crystals (Cervera et al. 2001), acoustic metamaterials (Guenneau et al. 2007), and acoustic resonators (Molerón, Serra-Garcia, and Daraio 2014) have also been used in the implementation of acoustic lenses. Further, another type of acoustic lens, which is proposed to be used in High Intensity Focused Ultrasound (HIFU) techniques, bases its design on a double foci to maintain the aperture of a transducer while reducing the f-number and the depth of focus. In this way, tissue coagulation can be induced in a smaller volume (Jang and Chang 2016). It is also important to consider the Side Lobe Level (SLL) parameter in ultrasound beamforming, because this parameter influences the image resolution. Regarding this parameter, a new type of lens called a super-oscillatory acoustic lens has been developed. This type of lens is proposed for image diagnosis due to the fact that it can focus at great distances and can minimize the SLL parameter, achieving an improved resolution (Hyun et al. 2018).

A Fresnel Zone Plate (FZP), as a simple example of an acoustic lens, has been used in this study due to its dimension and its fabrication advantages (Farnow and Auld 1974; O'Shea et al. 2004; Zhang, Yin, and Fang 2009). FZPs are constructed alternating opaque and transparent acoustic rings and use the diffraction phenomenon to modulate and focus acoustic waves. These classic FZPs are also called Soret Zone Plates (SZPs) (Soret 1875). Calvo *et al.* developed and characterized an SZP for underwater ultrasounds, alternating opaque and transparent zones made of soft silicone rubber (Calvo et al. 2015a). Results showed a main lobe widening, but also a small reduction on the first side lobes. Other studies show that acoustic field diffraction produces a maximum pressure field along the longitudinal axis. Nonetheless, secondary lobes can produce focal point resolution ambiguity (Bashford et al. 1997; Kanevsky 1977; Shimizu, Chubachi, and Kushibiki 1989).

In the ultrasound imaging technologies that require high resolution at the focus, the -3 dB main lobe width (R_{lat}) and the Depth of Focus (DoF) are the main factors that affect the quality of the image. In order to improve the lateral resolution (R_{lat}), it is necessary to increase the SLL, concentrating the energy at the focus and increasing the resolution. SZP lenses have a reduced DoF because they concentrate the energy in a much reduced zone along the longitudinal axis (Minin and Minin 2008). This can be a drawback in some applications, where a wider DoF is required. Moreover, SLL is rather poor in SZP lenses and could also be improved. For an arbitrary circular aperture at the focus, simplified expressions for lateral resolution, R_{lat}, and (DoF) are given by (Born and Wolf 2013):

$$R_{lat} = \alpha\lambda\frac{F_L}{D} = \alpha\lambda f^{\#} \tag{4.1}$$

$$DoF = \beta\lambda\left(\frac{F_L}{D}\right)^2 = \beta\lambda f^{\#2} \tag{4.2}$$

where α is the light gathering angle, β is light diffraction angle, λ corresponds to the wavelength, F_L is the focal length, D is the diameter of the lens, and $f^{\#}$ is the f-number, defined as the ratio of the focal length to the lens diameter. The β parameter is typically two in these lenses (Born and Wolf 2013; Minin and Minin 2004). Equation (4.1) is also valid in the focal area for a focused lens with a high numerical aperture (Minin et al. 2007). One could see that depending on the choice of frequency and $f^{\#}$, the lateral resolution can vary

over several orders of magnitude. Combining Equations (4.1) and (4.2), a relation between R_{lat} and DoF is obtained:

$$DoF = \frac{\beta}{\alpha^2 \lambda} R_{lat}^2 \qquad (4.3)$$

If conventional lenses are used, it is impossible to increase the DoF and the lateral resolution at the same time, as follows from Equation (4.3). For this reason, many papers investigated acoustic Bessel beams. The central core spot size of the Bessel beam is determined by the zeros of a Bessel function. If Bessel beam-based lenses are used, DoF and R_{lat} become independent parameters, as shown in Equations (4.4) and (4.5).

$$R_{lat} = \frac{2.4048}{k_r} = \lambda \frac{2.4048}{2\pi\beta} \qquad (4.4)$$

$$DoF = Z_{max} = \frac{D}{2\tan\beta} \qquad (4.5)$$

Thus, the R_{lat} does not depend anymore on the lens diameter. On the other hand, DoF depends on the diameter of the lens and the diffraction angle (McGloin and Dholakia 2005).

A flat acoustic lens with an aperiodical structure that transforms a divergent beam into a Bessel-like beam has been reported in (Xu et al. 2017). Bessel beams of sound waves have also been reported (Hsu, Margetan, and Thompson 1989; Jian-Yu Lu and Greenleaf 1994). However, they are not as broadly applied in acoustics as in optics, which is perhaps related to the lack of convenient formation techniques of such a kind of acoustic wave. Acoustic Bessel beams have been excited using acoustical axicons (Katchadjian et al. 2010), in analogy to the optical case. In any case, the most convenient way to form acoustic Bessel beams is by using annular transducer arrays (Masuyama et al. 1999; Masuyama and Mizutani 2006). The formation of an acoustic Bessel-like beam by using an axisymmetric grating of rigid tori was reported in (Jiménez et al. 2014). It could be mentioned that if Babinet's principle is considered, both approaches (SZP and rigid tori scatterers) are considered equivalent.

This work is based on the study carried out by Minin et al. in the field of electromagnetism (Minin and Minin 1990) (see Equation (4.7)). In that study, a modification of the distribution of the energy at the focus was proposed.

The authors showed that by choosing a reference radius smaller than the first FZP radii, the SLL ratio was improved (Webb, Minin, and Minin 2007; Minin and Minin 2011b). These results have been transferred to the ultrasonic field (Tarrazó-Serrano et al. 2019). Besides, the concept of the reference radius was independently used in acoustics (Clement, Nomura, and Kamakura 2015), but without analyzing the image quality. When a reference radius is larger than the first radii of the SZP equal to the equivalent design, this can be expressed as an SZP lens with a pupil mask, with the radius length equal to the reference radius (r_0).

The present work proposes and proves a new technique for acoustic quasi-Bessel beam formation using a planar structure based on SZPs (Soret 1875) by adding a Pupil mask to the SZP (PSZP). This PSZP presents an elongated focus while improving the R_{lat} simultaneously. Although SZPs in general and PSZP in particular are designed for a specific operating frequency, it has been demonstrated that SZP can also work at a range of different frequencies around the design frequency. In this case, there is a linear dependence between the focus location and the operation frequency (Fuster et al. 2017). Therefore, they could be used for imaging and therapeutic applications. It can be affirmed that, under specific conditions, part of a diffracted wave collimates, producing an elongated focus. Numerical calculations using the Finite Element Method (FEM) of acoustic waves propagating through such lenses were used to observe the complete acoustic field.

4.3 Mathematical Method and Simulations

SZPs are based on ring sections known as Fresnel regions. The purpose of the opaque rings is to block the destructive contributions to the focus. SZPs' building parameters are the focal length (F_L), the number of Fresnel zones (N), and the wavelength of the signal (λ). The following equation provides the Fresnel lens radii for plane wave incidence (Calvo et al. 2015a):

$$r_n = \sqrt{n\lambda F_L + \left(\frac{n\lambda}{2}\right)^2} \quad n = 1, 2, 3, ..., N \qquad (4.6)$$

In order to design the size of the pupil, the reference radius (r_0) has been introduced in the construction equation of the Fresnel lens. This is arbitrarily defined, taking into account that, from the point of view of geometrical optics, the properties of the zone plate are not modified (Minin and Minin 1990).

Nevertheless, this parameter is equivalent to modifying the reference phase in the wave approximation (Minin and Minin 2011b) and introduces the quasi-Fresnel radii concept. These radii are defined, for incident plane waves, by the following equation:

$$r_n = \sqrt{n\lambda\sqrt{F_L^2 + r_0^2} + \left(\frac{n\lambda}{2}\right)^2 + r_0^2} \; n = 1, 2, 3, ..., N \qquad (4.7)$$

The study of the physical phenomena involved in the interaction between the lenses and the wave front requires a mathematical model that considers the boundary conditions of the problem. In the present work, FEM has been implemented using the commercial software COMSOL Multiphysics (Multiphysics 2012) to calculate the acoustic pressure distribution. This method generates a numerical solution by discretizing the model and solving the Helmholtz partial differential equation:

$$\nabla \cdot \left(-\frac{1}{\rho_0}(\nabla p)\right) = \frac{\omega^2 p}{\rho_0 c^2} \qquad (4.8)$$

where ρ_0 is the host medium density, c is the ultrasound velocity, ω is the angular frequency, and p is the acoustic pressure. One of the problems with the use of FEM, is the extensive usage of memory resources, and axisymmetric models have been considered to optimize these limitations. The axisymmetric model takes into account the problem geometry, simplifying the model and reducing the computational time. Underwater transmission was considered with sound speed propagation ($c = 1500$ m/s) and water density ($\rho_0 = 1000$ kg/m^3). The wavelength of the signal (λ) was 6 mm, which corresponds to a design frequency (f) of 250 kHz. This λ has been selected to ease the mechanization of the lenses in the experimental setup. Lenses have been modeled as fully rigid considering the Neumann condition, which specifies that the sound velocity at the boundary was zero. The exterior contours of the model emulate the Sommerfeld condition. This boundary condition avoids internal reflections. Mesh geometry was fixed in triangles with a minimum element size of $\lambda/14$ and a maximum element size of $\lambda/8$ to prevent numerical dispersion.

In the current paper, lenses with high numerical aperture (NA) have been selected (NA$= 1/2f^{\#} = D/2FL = 2.5$). The focusing profile of this device ($F_L = 4.5\lambda$) presents a very compact beam with a short working distance. Figure 4.1 shows the normalized intensity maps and the axial focusing pro-

files for an SZP and a PSZP. Axes have been normalized with respect to the wavelength.
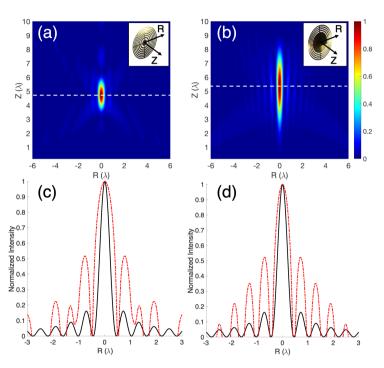
Figure 4.1: Self-normalized intensity maps to the maximum with the R-axis and the Z-axis normalized to λ for (a) a Soret Zone Plate (SZP) and (b) an SZP with amplitude Pupil mask (PSZP). Normalized intensity level focus transversal cuts from intensity maps (red dashed line) are compared to the Bessel J_0^2 function (black solid line) for (c) SZP and (d) PSZP.

It can be observed from Figure 4.1a,b that the SZP and PSZP lenses present focusing profiles with different focal lengths and shapes. As expected, the PSZP has a more extensive focus area (larger DoF) than the SZP. Moreover, the PSZP has a characteristic structure similar to quasi-Bessel beams with intensity profiles that closely resemble the ideal J_0^2 transverse-intensity distribution of Bessel beams (Figure 4.1d), while SZP does not show this behavior.

The normalized intensity distributions along the longitudinal axis (Z-axis) and the radial axis (R-axis) are presented in Figure 4.2. It can be observed that a maximum normalized intensity value is obtained in the SZP case, the PSZP maximum value being equal to 0.76.
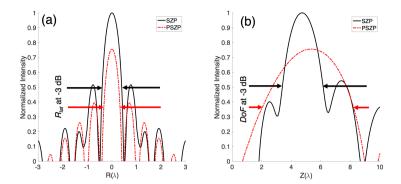
Figure 4.2: Numerical normalized intensity results for (a) the R-axis cut and (b) the Z-axis cut. The black solid line corresponds to classical Soret Zone Plate (SZP). The dashed-dotted red line corresponds to the amplitude pupil masked Soret Zone Plate (PSZP). Black and red arrows mark the DoF and R_{lat} limits for SZP and PSZP, respectively.

Table 4.1 shows DoF at -3 dB and R_{lat} at -3 dB for both SZP and PSZP lenses. As can been observed from Table 4.1, DoF in PSZP is larger than in a classical SZP, while the resolution for point objects in the PSZP is better since the central maximum is narrower and it has a little more energy in the outer rings of the diffraction pattern compared to the central maximum. Therefore, the PSZP generates quasi-Bessel beams increasing the DoF and reducing the diameter of the central spot when the pupil mask becomes larger. It is worth mentioning that a paraxial study of this phenomenon in the optical field was performed (Born and Wolf 2013). In the PSZP case, when the pupil becomes larger and more Fresnel zones are covered, the focus sharpens further in the radial direction, and the relative side lobe intensity is increased. Thus, the central zones play an important role in reducing the SLL, while the outer zones cause the central peak to sharpen. The diameter of the central maximum at the focal spot is less than the equivalent Airy disk. The DoF at -3 dB is the Full Length Half Maximum (FLHM) in the longitudinal axis, while R_{lat} at -3 dB is equivalent to the FLHM along the transverse axis.

The effects of extended DoF with a quasi-Bessel structure for PSZP may be described (to simplify the problem) as presented in Figure 4.3. The SZP lens consists of concentric dielectric rings, which can be treated as quasi-periodic gratings with different local grating constants at different radii. For single-point focusing, the normal incident wave is diffracted towards the designed focal point by these local gratings. The diffraction angles corresponds to the different radii and ensure the formation of a focal spot (Figure 4.3a). The

Table 4.1: Numerical values of Side Lobe Level (SLL) and Full Width Half Maximum (FWHM) for different values of the reference radius. Note that $r_0 = 0$ corresponds to SZP and the FWHM is obtained along R-axis.

	DoF at -3 dB (λ)	R_{lat} at -3 dB (λ)
SZP	2.84	0.81
PSZP	5.94	0.64
Bessel J_0^2	-	0.64

normalized radial spatial frequency k_r/k is related to the angle β as $k_r/k = \sin\beta$, where k_r is the radial component of the wave vector k and β is the angle between the wave vector and the longitudinal axis. For an ideal Bessel beam, the values of k_r and β are the same for all contributions. The range of the diffraction angle corresponds to the normalized angular spectrum bandwidth.
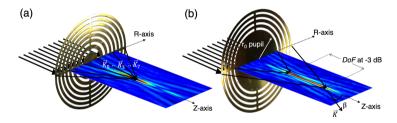
Figure 4.3: Beam formation scheme of (a) SZP and (b) PSZP.

A PSZP can also be described as diffraction gratings because the Fresnel zones' widths are almost identical. Thus, the local gratings diffract the incident waves towards different points on the longitudinal axis for a small range of diffraction angles (Figure 4.3b). The interference pattern is a 2D Bessel function of the first kind, located at the focal distance. Therefore, the local grating constant $d(r)$ at radius r can be obtained using the grating equation, $d(r)\sin\beta(r) = \lambda$, where λ is the incident wavelength. Thus, the original SZP angular spectrum is controlled by the pupil mask size. It should be noted that the acoustic lens is immersed in water, producing a compressed angular spectrum according to the refractive index of a medium.

The focused wave is diffracted from the outer rings, and the first-order diffraction beams form the acoustical needle, which is similar to the formation of a

quasi-non-diffracting beam with conical lenses. It should be noted that in the optical case, the pupil mask method was used to block the light in the point-focusing super-oscillatory lens to achieve a DoF as high as 5λ to 20λ. However, the achieving of such an extended DoF was at the expense of a degradation in the focus lateral resolution (Qin et al. 2015; Roy et al. 2014).

4.4 Experimental Results

The purpose of this work is to prove that an SZP with a Pupil mask (PSZP) is able to increase the DoF, reducing at the same time the R_{lat}. To carry out the implementation of both lenses, Equation (4.6) and Equation (4.7) have been considered for SZP and PSZP, respectively. The material selected for their construction was brass due to its low transmission coefficient. A reduced transmission factor allowed the lens rings to behave as a material opaque to sound. The SZP was mechanized applying construction conditions previously mentioned (Figure 4.4a). To construct the PSZP, Equation (4.7), which introduces the reference radius (r_0), was applied. The selected r_0 corresponds to the pupil radius, which blocked three Fresnel zones. As shown in Figure 4.4b, to ease the mechanization procedure, the PSZP was not built in two different parts (lens and pupil mask). Instead, the PSZP was mechanized as a single piece including the radius pupil r_0, which blocked three Fresnel zones.
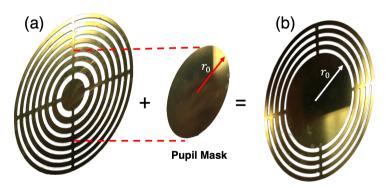
Figure 4.4: Implemented lenses in brass for the experimental results; where (a) corresponds to the experimental classical Soret Zone Plate (SZP) and (b) corresponds to the implemented Pupil masked Soret Zone Plate (PSZP).

All measures were done using an automated full-precision measurement system in order to validate and compare both lenses. This system consisted of a fixed

ultrasonic transducer and a 3D positioned hydrophone (Rubio et al. 2017), which granted precise and reliable results with 1×1 mm^2 scanning. The transducer used in this experiment was a 250 kHz Imasonic piston with 32 mm of active diameter, and the needle hydrophone was an MPM1/1 from Precision Acoustic Ltd. made of polyvinylidene fluoride with a diameter of 1.5 mm. A flat transfer function between 0.2 and 15 MHz provided the accuracy of the measurements.

Figure 4.5 shows the experimental self-normalized intensity maps for the SZP lens (Figure 5a) and the PSZP lens (Figure 4.5b). It can be seen that the pupil mask effect elongated the focus due to the diffraction grating lens behavior. In the SZP lens, as shown in Figure 4.5a, the focus was located at the designed F_L. In the PSZP case, the maximum energy was located at the same F_L as in the SZP case, but the energy was distributed along the longitudinal axis with a needle shape. The PSZP focused beam was also narrowed with respect to the SZP case.
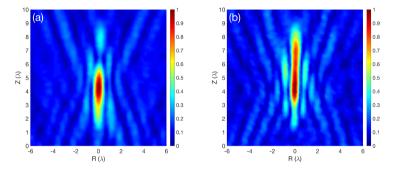
Figure 4.5: Experimental self-normalized intensity map results for the implemented lenses; where (a) corresponds to the experimental classical Soret Zone Plate (SZP) and (b) corresponds to the implemented Pupil masked Soret Zone Plate (PSZP).

The longitudinal and axial cuts for both lenses were obtained from intensity maps. The intensity cuts were normalized with respect to the maximum value and are shown in Figure 4.6 in order to highlight the differences in levels and energy distribution in both lenses. Figure 4.6a corresponds to the radial or R-axis cut. It can be observed that the decreasing of the secondary lobes was more similar to a Bessel function in the PSZP case than in the SZP case. Figure 4.6b corresponds to the longitudinal cuts of both lenses along the Z-axis. Here, it can be observed that the pupil mask generated a longitudinal energy distribution as opposed to the SZP behavior.
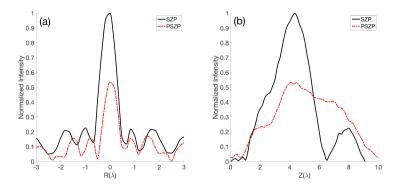
Figure 4.6: Experimental normalized intensity results for both implemented lenses. The axial and longitudinal axis are shown, where (a) corresponds to the R-axis cuts and (b) corresponds to the Z-axis cuts at the F_L position

Table 4.2 shows the experimental data obtained for the DoF at -3 dB and R_{lat} at -3 dB for both lenses. When DoF values were compared, an increase of 2.21λ was observed. Therefore, an expansion of the focus in the longitudinal axis was achieved. In the case of the R_{lat}, the PSZP achieved a narrower beam. The use of the pupil mask increased the resolution by 0.12λ. By comparing experimental and numerical values (see Table 4.1 and Table 4.2), it can be observed that there was a good agreement between them. The discrepancies found between Figure 4.2 and Figure 4.6 could be explained by the fact that the ultrasound transducer did not emit plane waves. In such a way, the wavefront arriving at the lens was not a completely plane wave.

Table 4.2: DoF at -3 dB and R_{lat} at -3 dB, comparison of the experimental results.

	DoF at -3 dB (λ)	R_{lat} at -3 dB (λ)
Experimental SZP	3.51	0.79
Experimental PSZP	5.72	0.67

4.5   Conclusions

In this work, we have proposed an improvement over a classical SZP intro-
ducing a pupil mask. The design of a quasi-non-diffracting beam with a sub-
wavelength transverse size was achieved using a PSZP. This design has been
verified using numerical models and experimental measurements in controlled
conditions. When an amplitude pupil mask was used, a quasi-Bessel beam was
obtained instead of a diffraction spot focus. This effect was produced by mod-
ifying the spherically-converging waves into quasi-conical waves. Therefore, a
quasi-Bessel beam distribution was obtained when a PSZP was used.

With the PSZP proposed in this paper, a spatial resolution enhancement from
0.81λ to 0.64λ was accomplished. In addition, DoF increased from 2.84λ to
5.94λ compared with the classical SZP. The experimental results were in good
agreement with the numerical simulations. The obtained results allowed the
modulation of the acoustic beam without modifying the lens. Therefore, the
same SZP could be used for different targets by changing the pupil mask, and
these results confer great versatility to SZP lenses. This type of PSZP has
applications in different areas where a compromise between DoF and lateral
resolution is required. As an example, in 3D imaging, ultrasonic sensors with
a long depth of focus eliminate the need for depth scanning, making this tech-
nique considerably faster.

Chapter 5

Tunable depth of focus of acoustical pupil masked Soret Zone Plate

5.1 Abstract

In acoustical lenses both resolution and depth of focus are determined by diffraction and the smaller the lens aperture the worse the resolution and the greater the depth of focus. Diffraction-limited resolution has a Soret Zone Plate, but a long depth of focus has an axicon. Nevertheless, these are two different devices each of which requires its own independent design. In this paper, we have shown that the transition from focusing to a diffraction limited spot to a quasi-diffraction free beam can be realized in the same focusing device

without changing its topology. It has been shown that using a classical planar Soret Zone Plate lens made of a concentric array of circular aperiodical rings with an amplitude pupil mask placed closely to the surface of lens allows to form a quasi-Bessel beams under specific conditions, part of a diffracted wave collimates, producing an elongated focus. Experiments were performed in water tanks in order to verify the simulation results. Experimental verification shown that the depth of focus of a pupil-masked Soret Zone Plate increases 1.63 times and resolution increases 1.2 times (with minimal beam waist about of 0.67 of wavelength and depth of focus about 5.72 of wavelength). By dynamically controlling the size of the amplitude pupil mask, it is possible to quickly control the depth of focus of an acoustic lens.

5.2   Introduction

Different ways for focusing and modulation of wavefronts have been researched by scientist and engineers because of its possibilities and applications in different physic areas. The applications of ultrasonic sensors are very varied ranging from their use to verify trees in poor condition, being a non-invasive technique (Goh et al. 2018), even to produce microfluidic movement by means of slightly focused acoustic waves (Zhu and Kim 1998). Zone Plates are one of these devices based on both refraction and diffraction mechanisms which can achieve wave focusing.

Zone Plates, which consist of alternating opaque and transparent Soret Zone Plates (SZP) or phase reversal Fresnel Zone Plates (FZP) rings (Rayleigh 1899; Soret 1875; Wood 1898; Fresnel 1996), are based on the diffraction phenomenon to modulate and focus acoustic waves, and as a simple example of acoustic lens has a long history (Yamada and Shimizu 1982; Yamada and Shimizu 1991; Farnow and Auld 1974) Acoustic Zone Plates have been used in different applications due to their flat surface, dimension and fabrication advantages (Schonbrun, Rinzler, and Crozier 2008; Amemiya et al. 1997; Minin and Minin 2011a). For example, self-focused acoustic ejectors using the double Fresnel Zone Plate were investigated (Hon et al. 2010). SZP for underwater ultrasounds alternating opaque and transparent zones made of soft silicone rubber was developed (Calvo et al. 2015b; Calvo et al. 2015a). Results had shown a main lobe widening but also, a small reduction of the first Side Lobe Level (SLL). Zone plate with fractal structures was studied (Castiñeira-Ibáñez et al. 2016). Acoustic Zone Plate lenses with extraordinary transmission based on Fabry-Perot resonances were investigated (Molerón, Serra-Garcia, and Daraio

2014). Modification of Zone Plate, which operates with piston emitters, was studied (Pérez-López et al. 2018).

However, relative small Depth of Focus (DoF) is one of the problems that SZP lenses have. To increase the depth of focus and spatial resolution many papers investigated so-called acoustic Bessel beams due to the central core spot size of the Bessel beam, which is defined from the properties of the zeros of a Bessel function. For example, with the help of an axicon, it is possible to form a Bessel beam of zero order (Kalosha and Golub 2007), whose central spot diameter at the half-wave intensity (Full Width at Half Maximum, FWHM) is equal to:

$$\text{FWHM}_a = \frac{0.36\lambda}{\text{NA}} \tag{5.1}$$

The resulting focusing spot will be about 30% smaller than the size of the Airy disk, formed by a lens with the same numerical aperture (NA):

$$\text{FWHM}_l = \frac{0.36\lambda}{\text{NA}} \tag{5.2}$$

Stratton originally proposed these Bessel beams in 1941 (Stratton 2007). Acoustic Bessel beams have been excited using refractive acoustical axicons (Burckhardt, Hoffmann, and Grandchamp 1973; Nagai and Iizuka 1982), in analogy to the optical case. Bessel beams of sound waves were also reported (Hsu, Margetan, and Thompson 1989; Katchadjian et al. 2010) and have been studied for realization with two-dimensional acoustic arrays (Jian-Yu Lu and Greenleaf 1994). In contrast to refractive axicon, diffractive flat axicon (Dyson 1958) has the same advantages as a flat Soret or Fresnel Zone Plates.

For example, a flat acoustic lens with aperiodical structure to transform a divergent beam into a Bessel like beam was reported (Xu et al. 2017). However, the most convenient way to form acoustic Bessel beams is by using annular transducer arrays (Jian-Yu Lu and Greenleaf 1994; Masuyama et al. 1999). Recently, the acoustic Bessel-like beam by means of an axisymmetric periodical grating of rigid tori was also reported (Jiménez et al. 2014), but it could be mentioned if Babinet's principle (Babinet 1837) is considered, both approaches (SZP and rigid tori scatterers) are considered equivalent. Thus, today acoustic diffraction flat lenses and axicon are successfully used in different applications. Nevertheless, these are two different devices each of which requires its own independent design.

In this paper, we propose and demonstrate that the transition from focusing to a diffraction-limited spot (lens with aperiodical structure) to a quasi-diffraction-free beam (axicon with periodical structure) can be realized in the same focusing device without changing its topology. We show a technique for acoustic Bessel-like beam formation using a classical planar Soret Zone Plate lens made of concentric array of circular aperiodical rings with amplitude pupil mask placed closely the surface of SZP. We show that, under specific conditions, part of a diffracted wave collimates, producing an elongated focus. Numerical calculations using Finite Element Method (FEM) of acoustic waves propagating through such a lens were used to observe the complete acoustic field. Finally, the experimental verification of quasi-Bessel beam formation by two type of SZPs is reported.

5.3 Methodology

To simplify the problem without loss of generality, geometrical optics interpretation is considered (Figure 5.1).
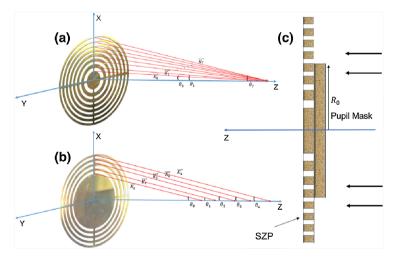
Figure 5.1: Ray-tracing for SZP (a) and PSZP (b). Combination of pupil-mask and SZP (c).

As it well-known binary SZP lens consists of concentric ring, which can be treated as a quasi-periodic grating with different local grating constants at different radii. For point focusing, the normal incident wave is diffracted towards

the designed focal point by these local gratings. The diffraction angles change in order to ensure the formation of a focal spot (Figure 5.1a). In this content SZP with pupil mask (PSZP) may be also considered as ring gratings because of the widths of transparent zones are almost constant while the pupil is blocking a central part of SZP. Thus, the local gratings diffract the incident waves towards different points on the optical axis with a small range of diffraction angle (Figure 5.1b).

For axicon (Dyson 1958) due to the diffraction angle (θ) of the ring grating and the grating period (P) are related by the Bragg's law: (Bragg and L. 1913) $P \cdot \sin(\theta) = m\lambda$, where m is the diffraction order and λ is the incident wavelength of acoustic wave, it produces Bessel beam. In the case of SZP with pupil mask, whose local periods P_i are not regular, we block those rings that can not be considered as periodic, and we may write that local $P_i = \Delta r_i$, where Δr_i is a width of i-th transparent zone and due to Δr_i is almost constant, and thus diffraction angles (θ_i) also almost constant, such pupil-masked SZP also will produce a quasi-Bessel beams.

When choosing the size of the pupil mask there is a compromise. On the one hand, the period and size of the slits should be as close to the periodic as possible. On the other hand, it is necessary to leave as many zones as possible on a fixed diameter of the lens in order to provide a sufficient length of focus. We settled on the criterion when the differences between neighboring zone width ($\Delta r_{i+1} + \Delta r_i$) is less than the $\lambda/5$ (Figure 5.2).

To verify the above-mentioned idea and simulate the acoustic pressure distribution in axisymmetric models of SZP we used the commercial software COMSOL Multiphysics with FEM method (Multiphysics 2012). Underwater transmission is considered with typical water values of sound speed propagation ($c = 1500$ m/s) and density ($\rho = 1000$ kg/m³). Design frequency (f) is 250 kHz, therefore wavelength (λ) is 6 mm. Lenses were defined full rigid considering Neumann condition. Mesh geometry was selected in triangles with minimum element size of $\lambda/14$ and maximum element size of $\lambda/8$ to prevent numerical dispersion.

The SZP lenses with high NA = 2.5 was selected (the NA is determined by both the diameter of the lens and the specified primary focal length as NA $= D/2F_L$) due to focusing of this device with $F_L = 4.5\lambda$ leads to a very compact beam with a short working distance. It could be noted that we can't use the well-known equations for NA due to small focal distance where the paraxial approximations are not valid. Analysis of the simulations shown that the focused field in the cases of PSZP (Figure 5.3b) insted of classical SZP
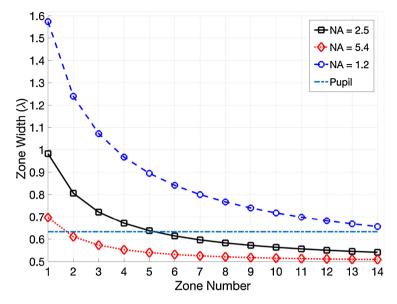
Figure 5.2: Zone width vs. number of transparent zones for different NA varying of focal length. Dash-dotted line is located at the value where the difference of zone width is less than $\lambda/5$.

(Figure 5.3a) has a characterisic structure for quasi-Bessel beams with intensity profiles that closely resemble the ideal J_0^2 transverse-intensity distribution of Bessel beams (see the inset in Figure 5.3b). FWHMs for these acoustical lenses are as follows: SZP 0.84λ, Bessel beams 0.64λ. Accordingly, the $DoFs$ are: for SZP 2.84λ and for PSZP 5.94λ.

5.4   Experimental Results

In order to carry out the experimental measurements, the SZPs were implemented in brass using a mechanization process. The material selected for its construction is brass because it has a relatively low transmission coefficient and behaves as an opaque sound material as shown in Figure 5.4. All the measures were done using an automated full precision measurement system in order to validate and compare the proposed lenses. This system consists of a fixed ultrasonic transducer and a 3D positioned hydrophone (Rubio et al. 2017) as shown in Figure 5.4. This system grants precise and reliable results with 1 mm × 1 mm scanning. The transducer used is a 250 kHz Imasonic piston
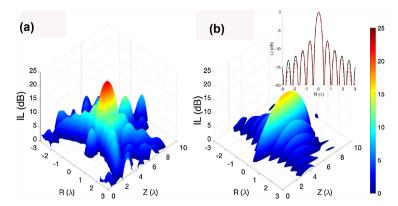
Figure 5.3: Acoustic intensity distributions near the focus of SZP (a) and PSZP (b). Inset in (b) shows axial comparison between J_0^2(black) and pupil mask (dashed line). (For interpretation of the references to color in text/this figure legend, the reader is referred to the web version of the article.)

with 32 mm of active diameter and the needle hydrophone is a MPM1/1 from Precision Acoustic Ltd. made of polyvinylidene fluoride with a diameter of 1.5 mm.

To ensure the far field condition, the distance between the transducer and the Zone Plate Lens was 0.4 m. Flat transfer function between 0.2 and 15 MHz provides accuracy on the measurements. Figure 5.5 shows the normalized by the maximum intensity planes for SZP and PSZP respectively. Experimental results are in good agreement with the numerical predictions. As it seen from the Figure 5.5b, the consideration of a ppil mask generates a distribution of energy along the longitudinal axis narrowing the beam and generating a quasi-Bessel beam distribution. Analysis of simulations and experimental investigations show that by adding an amplitude pupil mask shielding the central part of the lens, the focusing properties of the Soret lens dramatically change the field structure in the focusing region becomes close to the Bessel beam.

Experimental verification confirm that the depth of focus increase to 1.63 times and resolution increase to 1.2 times (with minimal beam waist about of 0.67λ and depth of focus about 5.72λ). It could be noted that in optical band central pupil mask method was used to block the light through the central part in the point-focusing super-oscillatory lenses to achieve a DoF more than 5λ; however, the realization of such an extended DoF was at the expense of degradation in the focus transverse size (Roy et al. 2014; Qin et al. 2015).
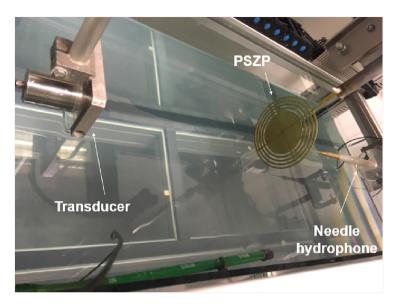
Figure 5.4: Experimental set-up. Assembly placed in a water tank for using the ultrasonic immersion transmission technique.

5.5 Conclusion

In this paper, it is shown that the focusing properties of an acoustic binary Zone Plate can be controlled without changing the structure of the zones by introducing an amplitude pupil mask. In this case, diffraction by a quasi-periodic ring lattice formed by peripheral Fresnel zones leads to the formation of an elongated focus corresponding to the structure of a quasi-Bessel beam. The depth of focus is determined by both the size of the pupil mask and the diameter of the acoustic lens. Therefore, circular gratings based on pupil-masked SZP, will enable an intense quasi-Bessel beam with diffraction limit waist and much extended DoF. By dynamically changing the size of the amplitude pupil mask, it is possible to quickly control the depth of focus of the acoustic Soret lens.

Experimental verification shows that the depth of field increases to 1.63 times and resolution increase to 1.2 times (with minimal beam waist about of 0.67λ and depth of focus about 5.72λ). Such systems can find wide application in nondestructive devices, acoustic microscopy, imaging systems and control of nano and micro particles. The extremely easy generation of these beams
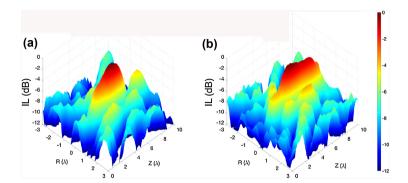
Figure 5.5: Experimental normalized by the maximum intensity 3D planes for (a) SZP and (b) PSZP.

using pupil binary mask proposed here can handle high wave powers, thus is particularly suitable for applications in plasma channel generation, nonlinear optics, and X-ray or microwave beam manipulation. Moreover, this approach can also be directly applied to light and matter waves.

Chapter 6

MRI Compatible Planar Material Acoustic Lenses

6.1 Abstract

Zone plate lenses are used in many areas of physics where planar geometry is advantageous in comparison with conventional curved lenses. There are several types of zone plate lenses, such as the well-known Fresnel zone plates (FZPs) or the more recent fractal and Fibonacci zone plates. The selection of the lens material plays a very important role in beam modulation control. This work presents a comparison between FZPs made from different materials in the ultrasonic range in order to use them as Magnetic Resonance Imaging (MRI) compatible materials. Three different MRI compatible polymers are

considered: Acrylonitrile butadiene styrene (ABS), polymethyl methacrylate (PMMA) and polylactic acid (PLA). Numerical simulations based on finite elements method (FEM) and experimental results are shown. The focusing capabilities of brass lenses and polymer zone plate lenses are compared.

6.2 Introduction

The development of modulating and focusing energy systems has been a field of study of great interest for scientist and engineers. The lens is a devices that is able to perform this energy modulation. Lenses allow beam forming, control propagation and focusing the energy that impinges on them. These effects are produced by refractive and diffractive phenomena. Transmission efficiency is one of the most important aspects, particularly when low impedance contrast is presented between the lens and the host medium. Due to the wide versatility of the lenses, they have been used in different areas. For example, they have been applied in sonochemistry (Li et al. 2003) , construction (McCann and Forde 2001) and the pharmaceutical industry (Albu et al. 2004).

The acoustic lenses, depending on the physics involved in the beam formation, can be divided into different groups, including refractive lenses and diffractive lenses. One example of lenses based on the refraction phenomenon are sonic crystal lenses made of periodic distributions of rigid cylinders (Cervera et al. 2001). Due to the subsonic sound speed inside the crystal, these lenses act similar to those in optical systems. Another example of this typology of acoustic lenses are those which modify the refractive index using labyrinths. These type of lenses are the so-called Gradient-Index lenses (Li et al. 2012; Welter et al. 2011; Peng, Xiao, and Wu 2014).

The other subtype of lenses, based on the diffractive phenomenon, conducts its behavior on the constructive interferences of the pressure field. An example of these types of lenses is the fractal lenses, which are able to generate different foci depending on their fractal geometrical properties (Castiñeira-Ibáñez et al. 2018). Fresnel Zone Plates (FZP) have an improved focusing capacity. Among the different ways to implement FZPs, one of the most common and easiest is to alternate transparent and blocking zones, which results in a Soret type FZP (Soret 1875). To obtain these blocking areas, materials that are opaque to sound are required. This fact is accomplished by selecting materials that have a high impedance contrast with the host medium. There are studies that have implemented Soret FZP (SZP) by ultrasounds based on these type of lenses (Calvo et al. 2015a).

A material that has a high impedance with respect to water and that allows for the creation of opaque zones to achieve a Soret type lens is brass. However, this type of material has limitations, especially when used in fields such as bioengineering. The use of acoustic lenses in medicine for high intensity focused ultrasounds (HIFU) treatment is one of the current lines of research. Magnetic Resonance Imaging (MRI) is the technique that is most used for guiding HIFU treatment (McDannold et al. 1998).

MRI is a technique used for soft tissue structure imaging in a non-invasive way. The image is obtained by aligning and relaxing the magnetic moments of the atoms of the introduced elements in the MRI. Tissues are exposed to a strong external time-independent magnetic field. Thus, metallic elements cannot be introduced in the resonance zone due to their interference in the image and because they could damage MRI-systems. To avoid interaction with the electromagnetic field, non-metallic materials should be used in the construction of lenses. One of these materials is polylactic acid (PLA) (Drumright, Gruber, and Henton 2000). The MRI environment requires materials such as PLA for medical instruments and patient supports. Recently, PLA has been used for this purpose and its reliability has been shown (Herrmann et al. 2014). The HIFU transducer is embedded within a specially designed table that fits into the MRI device. This integrated system, has a degassed water bath where the transducer is located. The patient lies over this system on (Köhler et al. 2009). Although the transducer and the lens must be immersed in this water bath, degradation of the PLA will occur over long-term immersion. PLA degrades in water after a period ranging from months to a year (Rocca-Smith et al. 2017). Therefore it must be taken into account that, in MRI systems, the lens and the transducer are not permanently submerged. After 20 to 25 min, the system is extracted from the water bath, and for this reason, the time of degradation due to being immersed in water can be prolonged considerably.

In this work, three lenses with three types of compatible materials with MRI environments are compared. In this sense, acrylonitrile butadiene styrene (ABS), polymethyl methacrylate (PMMA) and polylactic acid (PLA) materials are used. Furthermore, a SZP built in brass is compared. Although, this material is not MRI compatible, it is the nearest to the ideal SZP that can be implemented in real projects. In the comparison, a not compatible with MRI lens built in brass and an ideal Soret lens will be added. Results are obtained and compared both numerically and experimentally. Numerical results have been obtained using the commercial software COMSOL Multiphysics 4.3a by COMSOL Inc. (Sweden) (Multiphysics 2012). In this work, it has been verified that

the ratio of the transmission capacity that is related to the ratio of impedances of the medium and the lens, directly influences the focusing capacity.

6.3   Methodology and Theoretical Analysis

Fresnel zone plates are circular concentric structures, which are known as Fresnel regions. Every consecutive region has a π phase shift between them. This fact makes a coherent contribution to obtain high intensity levels at focal length (F_L), which is the location in the axial coordinate where the focus is placed. The number of Fresnel regions is defined as N, this includes both opaque and transparent acoustic sections. The working frequency is defined as f and radial distances (r_n) of each Fresnel zone can be obtained using Equation (6.1) valid for plane wave incidence.

$$r_n = \sqrt{n\lambda F_L + \left(\frac{n\lambda}{2}\right)^2} \tag{6.1}$$

In this work, underwater transmission is considered and lenses are designed for ultrasound applications. Therefore, piston sources have to be considered when FZPs are implemented. Due to spherical wave incidence consideration, Equation (6.2) has been used where d is the separation between the point source and the lens.

$$d + F_L + \frac{n\lambda}{2} = \sqrt{d^2 + r_n^2} + \sqrt{F_L^2 + r_n^2} \tag{6.2}$$

The acoustic wave has to propagate through the host medium, then cross Fresnel regions and afterwards continue through the host medium. A three-layer configuration has to be considered (Figure 6.1). Acoustic impedance (Z) is defined as the product of the medium density (ρ) and the sound propagation velocity (c) in it. Therefore, it is necessary to consider the input (Z_{in}) and output (Z_{out}) acoustic impedance and the transmission pressure coefficients must be calculated (t). This coefficient is a clear indicator of the blocking capacity of the elements of the FZP. Hence, t is defined as the relation between the transmitted field and the incident field. Density (ρ), sound propagation velocity (c) and acoustic impedance (Z_{mat}) values have been shown in Table 6.1 . Using these values in Equation (6.3), Z_{in} could be obtained (Kinsler et al. 1999).

$$Z_{in} = Z_{mat} \frac{Z_{out} + jZ_{mat} \tan k_{mat} d}{Z_{mat} + jZ_{out} \tan k_{mat} d} \tag{6.3}$$

Where k_m is the wave number, defined as $k_m = \omega/c$. Considering $\omega = 2\pi/f$. Once Z_{in} is obtained, reflection coefficient is defined in Equation (6.4).

$$r_{in} = \frac{Z_{in} - Z_{water}}{Z_{in} + Z_{water}} \tag{6.4}$$
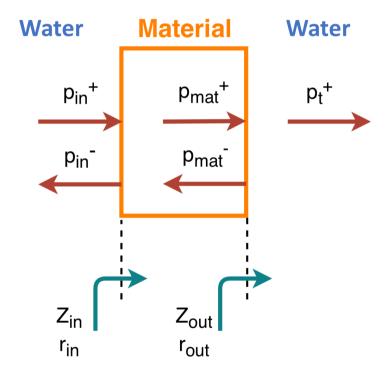
Figure 6.1: Transmission diagram of the implemented lenses.

The equation that relates the field balance as a function of the impedance and reflection coefficient of the system is defined in Equation (6.5) and gives t values depending on the material.

$$|t| = \frac{|p_t^+|}{|p_i^+ n|} = \sqrt{(1 - |r_{in}|^2)} \tag{6.5}$$

Table 6.1: Density and sound speed values. Acrylonitrile butadiene styrene (ABS), poly-lactic acid (PLA), and polymethyl methacrylate (PMMA).

Material	ρ (kg/m^3)	c (m/s)	Z_{mat} (Rayls)	Z_{mat}/Z_{water}
ABS	1050	2250	$2.4 \cdot 10^6$	1.58
PLA	1240	2220	$2.8 \cdot 10^6$	1.84
PMMA	2690	1191	$3.2 \cdot 10^6$	2.14
Brass	8400	4700	$39.5 \cdot 10^6$	26.32
PLA-Air-PLA	398	944	$3.6 \cdot 10^5$	0.25

Considering the transmission coefficient values obtained (0.23 for brass, 0.51 for PLA-Air-PLA and more than 0.95 for ABS, PLA and PMMA), it can be affirmed that full implemented MRI compatible material lenses will focus less energy at the F_L if it is compared to brass FZP or ideal SZP. Therefore, one solution is proposed to obtain the desired impedance contrast. A FZP that includes an air chamber inside the structure has been implemented by using a 3D-printer. Thus, both lenses, full-PLA and air-chamber, have been compared.

6.3.1 Numerical Model

The finite elements method (FEM) was used to obtain a numerical solution of the physical problem. The finite elements method allows us to study the physical phenomena involved in the interaction of waves with FZPs. Therefore, a mathematical model that replicates the conditions of the problem was implemented. This method also allows us to determine the pressure distribution of the diffracted fields generated by the FZP when there is a piston emitter, causing interference phenomena. From the mesh generated by FEM, a partial differential equation solution was obtained for each node (Zienkiewicz et al. 1977). In this case, acoustic Helmholtz equation is considered (Equation (6.6)). To solve the Helmholtz equation, standard values of water such as density of the medium ($\rho = 1000$ kg/m^3) and sound propagation velocity ($c = 1500$ m/s) have been considered. The working frequency of the FZPs was 250 kHz and it can be found by its relation with the angular velocity (ω). Finally, p corresponds to the acoustic pressure.

$$\nabla \cdot \left(-\frac{1}{\rho_0}(\nabla p) \right) = \frac{\omega^2 p}{\rho_0 c^2} \tag{6.6}$$

If a 3D model is considered, this will require high computational resources. To simplify the model and reduce this computational cost, as shown in previous works (Castiñeira-Ibáñez et al. 2016; Tarrazó-Serrano et al. 2019), the geometrical properties of the model were used taking advantage of its axisymmetry. Therefore, the model was simplified by implementing a semi-lens only. A complete solution is obtained by rotating it from its symmetry axis. This procedure achieves a reduction of the degrees of freedom necessary to obtain the results of the numerical simulation and thus significantly diminishing the calculation time.

The boundary conditions defined in the numerical models were explained below as seen in Figure 6.2. The contours of the model were defined as wave radiation condition boundary to emulate an infinitely large medium and therefore the Sommerfeld condition was satisfied. Acoustic impedance domain definition were used for all opaque Fresnel regions for each lens. In the case of the SZP lens, the contours were considered infinitely rigid, applying the Neumann condition (the sound velocity in the contour is zero).
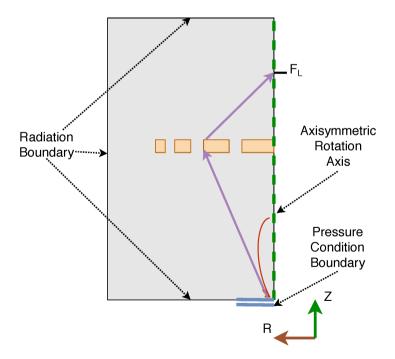
Figure 6.2: Scheme of the finite element method (FEM) conditions.

6.4   Experimental Set-Up

It is required to validate the results obtained from the theoretical models with other solutions such as numerical models and experimental measurements. In this sense, obtaining experimental results is fundamental to validate the numerical models. A complex measurement and acquisition system is needed to perform the experiments given the technical difficulties to control the underwater devices. The Center for Physics Technologies: Acoustics, Materials and Astrophysics of the Universitat Politècnica de València has a robotized and automated system for high precision ultrasound measurements. The robot is built based on the size of the immersion tank where the tests and experiments are carried out, which contains distilled and degassed water, with dimensions of 0.5 m wide by 0.5 m high by 1 m long. These dimensions suppose that the immersion tank must contain around 200 L of distilled water to be functional, and allow both transducers and devices to be completely submerged, and avoid reflections due to the impedance changes produced by the change medium.

The measurement system is composed by a fixed emitter and a hydrophone coupled to the robotic system. This system obtains reliable and precise results that allow for the evaluation of the acoustic phenomena involved in these types of lenses. A plane immersion piston transducer built by Imasonic with 250 kHz of central working frequency and an active diameter of 32 mm has been used as the emitter. Also, a Precision Acoustics hydrophone, model 1.0 mm Needle Hydrophone is used as the receiver. This hydrophone is capable of measuring high frequencies, even if they have a very weak signal level. The sensitivity of the hydrophone is 850 nV/Pa (-241.4 dB $1/\mu$Pa) with a tolerance of ± 3 dB. The frequency response is flat ± 2 dB between 3 and 12 MHz and ± 4 dB between 200 kHz and 15 MHz. The bandwidth ranges from 5 kHz to 15 MHz. Figure 6.3 shows an experimental set-up in a measurement. Two types of different configurations are used to generate and amplify the signals. The first one is to use an external function generator connected to a high power amplifier. The second configuration is to use a pulse generator (5077PR of Panametrics) with integrated amplifier. This generator and amplifier allows generating pulses with frequencies between 100 kHz and 20 MHz, a pulse repetition frequency (PRF) from 100 Hz to 5 kHz and a pulse amplitude between 100 and 400 V.

All the results shown below were obtained for a working frequency of 250 kHz. For the experimental comparison, three lenses were implemented, two made of PLA and one of brass. Every lens considered in this work was designed with 11 Fresnel zones and an outer radius of 88.8 mm. The thickness of the brass

Figure 6.3: Experimental set-up.

lens was 1 mm. For manufacturing reasons, the rest of the lenses had a total thickness of 5 mm. Figure 6.4 shows both PLA and brass lenses. Both PLA lenses were identical, the only difference being an inner air chamber to achieve a higher impedance contrast. As described in the previous section, it is not possible to differentiate them by the naked eye.
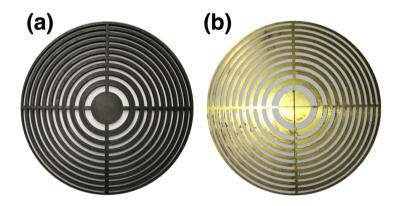
Figure 6.4: Implemented lenses, (a) PLA and (b) brass.

6.5   Results

Intensity gain for longitudinal axis cuts and maps have been calculated to compare all the lenses coherently. One parameter, which can be used to evaluate the focusing capacity of a lens is the intensity gain (G). The intensity gain is related with the intensity with both the intensity with lens (I) and intensity without lens (I_0), as shown in Equation (6.7).

$$G(dB) = 10 \cdot \log_{10}(I/I_0) \tag{6.7}$$

Intensity gain values have been calculated from Equation (6.7). Figure 6.5, shows the intensity gain for longitudinal cuts on the Z axis for both, numerical and experimental results. It can be seen from Figure 6.5a, that higher impedance contrast, as in the case of the ideal SZP or brass FZP lens, gives rise to a higher gain levels. As expected, the lower gains are obtained with those materials with impedance contrast values between 1 and 2 and for impedance contrast values lower than 1, the intensity gain increases. ABS, PLA, PLA-Air-PLA, and PMMA polymers, according with the values showed in Table 6.1, are not able to achieve enough intensity gain as brass FZP. By comparing the experimental results obtained for brass and PLA (see Figure 6.5b) with numerical ones (see Figure 5a) it can be seen that there is a good agreement. From Figure 6.5b, it is observed that the air chamber PLA lens has higher intensity gain than full PLA lens. This fact can be explained by the introduction of an air layer. This layer, due to its low acoustic impedance, can block the transmission of the ultrasonic waves approaching its behavior to an ideal SZP. Nevertheless, a focal length displacement of 1.66λ is observed in the FZP lens built with air chamber and PLA. In this case, the displacement is due to the new three-layer configuration (PLA-Air-PLA). The resolution of the 3D-printer and the wall width needed to avoid porosities means that there is an interface between the host medium and the air chamber.

Figure 6.6 shows four intensity gain maps, the first three obtained experimentally and the fourth numerically. The experimental ones correspond to PLA, PLA-Air-PLA and brass, while the numerical one has been obtained using an ideal SZP. It has been verified how the results obtained with brass resembles the ideal SZP. This is due to the rigidity of the material. On the other hand, in PLA lens results, a diminishing intensity gain is observed. This intensity gain level can be improved using a PLA-Air-PLA lens. All the lenses are designed with a focal length located at 8.33λ for a working frequency of 250 kHz. When the lens is able to block destructive interference, it is possible to locate the
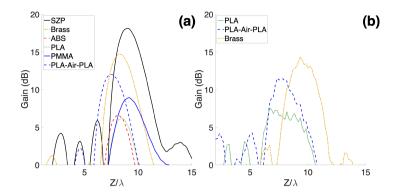
Figure 6.5: Intensity gain longitudinal cuts for (a) FEM results and (b) experimental results.

focus in F_L. This occurs in brass and the ideal SZP case. Resulting from the lack of blocking capability, the full PLA FZP could not impede the incident pressure wave transferal generating aberrations in the F_L.
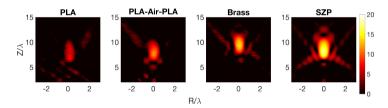
Figure 6.6: Intensity gain maps for experimental measurements and ideal SZP numerically obtained (FEM).

6.6 Conclusions

Non-metallic materials can be used for the construction of acoustic lenses. Three alternative materials, compatible with magnetic resonance, have been proposed instead of brass lenses. It has been possible to verify that the higher the impedance contrast of the materials, the higher the intensity gain levels. The PMMA lens has higher intensity level than ABS and PLA ones, because it has a slightly higer impedance contrast value than ABS or PLA. However, the use of an air chamber inside the PLA lens increases the intensity gain levels,

due to the fact that values of impedance contrast less than one means blocking of the waves. PLA is a biocompatible material and is cheaper than PMMA. 3D printers give open field of new lens design MRI compatible. Moreover, since PLA is a biodegradable material, it is a environmental friendly material. This point is important in procedures that generate waste. Nevertheless, the manufacture of PLA lenses require great care because of microporosities that could appear. The appearance of pores can cause water to enter into the lens, drastically reducing the blocking capacity. In addition, polymers such as PLA, ABS or PMMA are more affordable than metal plates. This will lower the costs in the production of HIFU treatment devices based on acoustic lenses. For this reason, PLA is proposed as an MRI compatible material with great potential for therapeutic applications of ultrasound focusing.

Chapter 7

Acoustic Focusing Enhancement In Fresnel Zone Plate Lenses

7.1   Abstract

The development of flat acoustic lenses for different applications such as biomedical engineering is a topic of great interest. Flat lenses like Fresnel Zone Plates (FZPs) are capable of focusing energy beams without the need of concave or convex geometries, which are more difficult to manufacture. One of the possible applications of these type of lenses is tumor ablation through High Intensity Focused Ultrasound (HIFU) therapies with real time Magnetic Resonance Imaging (MRI) monitoring. In order to be MRI compatible, the FZP material cannot have electromagnetic interaction. In this work, a Phase-Reversal FZP (PR-FZP) made of Polylactic Acid (PLA) manufactured with a commercial 3D printer is proposed as a better, more efficient and MRI compatible alternative

to conventional Soret FZPs. Phase-Reversal lenses, unlike traditional FZPs, take advantage of all the incident energy by adding phase compensation regions instead of pressure blocking regions. The manufactured PR-FZP achieves 21.9 dB of focal gain, which increases the gain compared to a Soret FZP of its same size by a factor of 4.0 dB. Both numerical and experimental results are presented, demonstrating the improved focusing capabilities of these types of lenses.

7.2 Introduction

One of the most important issues in the acoustics field is sound focusing due to its multiple applications. This focalization phenomenon is produced by acoustic lenses, which are devices capable of concentrating acoustic energy in a specific area. Acoustic lenses are used in many applications of different nature, ranging from medical applications for the diagnosis and/or treatment of medical pathologies, to non-destructive testing or food industry (Chen, Sharma, and Mudhoo 2011; Minin and Minin 2011a). This wide range of applications of acoustic lenses makes these devices a hot topic among the scientific community. Sound focusing can be achieved through diffraction or refraction phenomena. Thus, in the last decades, different designs of acoustic lenses have been devised, such as acoustic lenses based on phononic crystals (Cervera et al. 2001), gradient acoustic lenses that use space-coiling in their designs (Peng, Xiao, and Wu 2014; Wang et al. 2014) acoustic lenses that use Helmholtz resonators or metamaterial based split-ring type resonators in their designs (Yang et al. 2015) or acoustic lenses based on Fabry-Perot resonances in apertures (Lin et al. 2014). Now, the geometry and efficiency in the optimal design of an acoustic lens are crucial parameters for its subsequent application to different fields. An optimal design would be one in which the lens had a small size, flat geometry and great energy efficiency. In this sense, recent studies have developed small size and high transmission efficiency flat ultrasound lenses based on sandwiched layers of silicone and resin (Xia et al. 2018).

Acoustic lenses focus sound in the same way than optical lenses focus light, because the underlying theory is applicable to both mechanical and electromagnetic waves. The research and the devices obtained for the case of electromagnetic waves can be extended to acoustic waves. One of these devices, that originally was conceived to focus electromagnetic waves and that was later transferred to the acoustics field, is the Fresnel Zone Plate (FZP) lens. FZP lenses are formed by a set of concentric rings with decreasing width. Each ring constitutes a Fresnel region, and between two consecutive regions there is a π

phase difference. Based on this fact, two types of lenses can be distinguished: Soret type FZPs and Phase-Reversal FZPs (PR-FZPs). Soret type FZPs Soret 1875 alternate transparent with pressure blocking regions that reflect the pressure contributions that are in phase opposition with those of the transparent regions. Blocking regions are implemented with materials that have either a high impedance contrast with the host medium or a high attenuation constant, which ensures a high reflection and a low transmission coefficient, respectively. PR-FZPs Park et al. 2009 replace blocking regions with phase reversal regions that correct the phase of the pressure contributions by adding a π phase change that generates a constructive interference at the focal distance. This means that, unlike FZPs, with PR-FZPs all the regions of the lens and not only the transparent ones contribute constructively to the focal area, which ideally increases the lens efficiency and focal intensity by a factor of 4, as twice the pressure is focused into the focal distance.

In general, FZP lenses can be used for acoustic focusing in both air and water. In this sense, Shindel (Schindel, Bashford, and Hutchins 1997) and Welter (Welter et al. 2011; Welter et al. 2012) designed and presented experimental results on FZP lenses for their use in air. Subsequently, the concept of coiling up space, this is labyrinthine channels, was applied to the focusing of sound waves in air. Moleron *et al.* (Molerón, Serra-Garcia, and Daraio 2014) and Li *et al.* (Li et al. 2015) increased the efficiency of FZP lenses using labyrinthine channels in the opaque rings. In the case of underwater acoustic focusing, Calvo *et al.* (Calvo et al. 2015a) proposed a FZP lens with alternating transparent and opaque zones made of soft silicone rubber. Recently, studies about the influence of the reference radius or phase in the FZPs design have been carried out. Using this parameter in the implementation of FZP lenses, their focus properties can be modified (Castiñeira-Ibáñez et al. 2019). Moreover, side-lobe levels can be improved to obtain a better spatial resolution (Tarrazó-Serrano et al. 2019). Generally, when FZP lenses are used in air or water, these are manufactured using materials with a large impedance mismatch with the host medium, which is the main reason why metals are generally used for their implementation. One of the main uses of acoustic lenses in the medical field is tumor ablation through High Intensity Focused Ultrasound (HIFU) therapies. These therapies are usually guided in real time using MRI monitoring systems, which can provide an image of the temperature rise in the targeted cancerous tissue (Marsac et al. 2012). However, MRI systems are not compatible with metallic devices, which makes FZP implementations more difficult to achieve. Many of the compatible MRI commercial devices use PolyLactic Acid (PLA) as material (Herrmann et al. 2014). PLA is an Aliphatic Polyester derived from

100% renewable resources, versatile and biodegradable with reduced costs, and it is used in biomedical applications (Drumright, Gruber, and Henton 2000).

Commercial HIFU devices are either based on phased arrays or geometrically focused transducers (Ebbini and Cain 1991; Uchida et al. 2006). On the one hand, phased arrays offer high flexibility with dynamic control of the focal distance and beam width, although these devices are usually very expensive. On the other hand, focused transducers have lower cost compared to phased array solutions, but there is a lack of control in the focal distance, which can not be practical in some therapeutic situations. In this sense, FZPs are simpler options that allow to control both the focal distance and the beam width. The focal distance of FZPs can be dynamically shifted by tuning the working frequency (Fuster et al. 2017), while the number of Fresnel regions selected at the design stage of the lens controls the beam width.

Nowadays, acoustic FZPs are based on Soret type implementations, which focusing efficiency is low because half of the incident energy is reflected at the blocking regions. In this paper, we design, manufacture and experimentally validate a PR-FZP lens, which design is inspired in a phase-reversal zone plate (Rayleigh 1888). The PR-FZP, originally developed for electromagnetic waves, has been used as an antenna in the range of microwave and millimeter wave regions (Black and Wiltse 1987; Huder and Menzel 1988), and more recently as THz sieves for optical focusing applications (Machado et al. 2018). Knowing that we can extend the results obtained for electromagnetic waves to acoustic waves, an acoustic PR-FZP has been designed to increase the energy efficiency compared to conventional FZPs. In addition, it is made of a MRI compatible material, which makes the PR-FZP suitable for therapeutic ultrasound focusing applications. The acoustic PR-FZP has been manufactured using a commercial 3D printer and PLA. Both numerical and experimental results indicate excellent performance, obtaining gains at the focal region above 21.9 dB. Furthermore, due to it its low manufacturing cost and low weight, the designed PR-FZP offers great flexibility, becoming an appealing alternative to conventional HIFU devices.

7.3   Results

When a piston transducer is used as emitter, spherical wave incidence on the lens has to be considered. In the far field, the piston can be described as a point source emitter with a given directivity pattern, $D(\theta)$ (Kundu et al. 2010). The design equation of the FZP radii can be obtained considering a $\lambda/2$ increase between the pressure propagation paths of two consecutive regions, which is equivalent to a π phase increase. Thus, the radii can be calculated using the following expression (Calvo et al. 2015a; Pérez-López et al. 2018):

$$d + F_L + \frac{n\lambda}{2} = \sqrt{r_n^2 + d^2} + \sqrt{r_n^2 + F^2}, \tag{7.1}$$

Where d is the distance between the point source and the FZP, F_L is the focal distance, λ is the wavelength, r_n is the radius of each region and $n = 1, 2, 3, ..., N$, being N the total number of Fresnel regions.

Once the different radii are calculated using Equation (7.1), the FZP is obtained by alternating transparent regions with either pressure blocking (Soret FZP) or phase-reversal regions (PR-FZP). If a PR-FZP implementation is selected, the thickness of the phase-reversal regions has to be such that the phase difference introduced compared to transparent regions is an odd multiple of π. The phase difference is given by $\Delta\theta = |k_m - k_0|t_h$, where t_h is the thickness of the lens and $k_m = 2\pi/\lambda_m$ and $k_0 = 2\pi/\lambda_0$ are the wave numbers of the lens material and the host medium, respectively. Therefore, the thickness of the lens can be calculated as

$$t_h = \frac{q}{|k_m - k_0|}\pi = \frac{q}{2}\frac{\lambda_0\lambda_m}{|\lambda_0 - \lambda_m|} \tag{7.2}$$

Where $q = 1, 3, 5, ...$ is a design parameter that determines the thickness of all Fresnel regions.

Figure 7.1 shows a scheme of a PR-FZP placed at a distance d from a directional piston transducer. As it can be observed, the lens material introduces a phase shift to the incident pressure, which generates a constructive interference at the focal distance. Ideally, the pressure generated at the focal distance by a PR-FZP is twice the pressure generated by a conventional FZP because every Fresnel region of the lens contributes constructively at the focus. However, as depicted in Figure 7.1, in a practical case some of the incident energy is reflected at the lens material due to the impedance mismatch between the

material and the host medium, which means that the pressure at the focal distance, and therefore the lens efficiency, will be reduced compared to the ideal case. The impedance mismatch can be evaluated using the reflection coefficient, defined as $\Gamma = p_r/p_i$, with p_r and p_i being the reflected and the incident pressure, respectively. In the situation described in Figure 7.1, the reflection coefficient can be calculated using the following expression:

$$\Gamma = \frac{j\tan(k_m t_h)(Z_m^2 - Z_0^2)}{2Z_m Z_0 + j\tan(k_m t_h)(Z_m^2 + Z_0^2)} \tag{7.3}$$

Where $Z_m = \rho_m c_m$ and $Z_0 = \rho_0 c_0$ are the characteristic acoustic impedances of the lens material and the host medium, respectively. ρ_0, ρ_m, c_0 and c_m are the densities and sound propagation speeds of the lens material and the host medium.
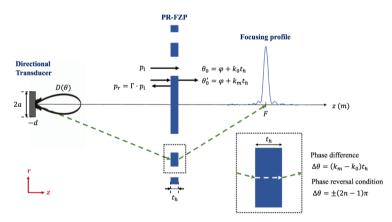
Figure 7.1: Schematic diagram of the Phase-Reversal Fresnel Zone Plate (PR-FZP)

The transmission coefficient, defined as $\tau = |p_t|/|p_i|$, where p_t is the transmitted pressure, can be calculated from the reflection coefficient as $\tau = \sqrt{1 - |\Gamma|^2}$. A low transmission coefficient would reduce the lens focusing capability. Thus, there are two design factors regarding the implementation of the phase-reversal regions: the lens material and its thickness. The lens material has to be selected in order to minimize the reflection coefficient, which maximizes the transmitted pressure through the phase-reversal regions. Once the material is selected, its thickness can be directly calculated using Equation (7.2), which provides the phase-reversal condition. In this sense, Figure 7.2a shows a comparison between the squared transmission coefficient of a lens made of PLA (blue line)

and a lens made of brass (red line) as a function of the material thickness. The host medium is water, and the working frequency is fixed to 1 MHz. Table Table 7.1 shows the acoustic properties of the considered materials. Figure 7.2b depicts the phase difference between transparent and phase-reversal regions for both materials. The horizontal black line represents the $\Delta\theta = \pi$ condition, while vertical dashed lines represent the thicknesses which fulfill the phase-reversal behaviour. As it can be observed, for the brass material, the π phase shift occurs at the thickness of 1.286 and 3.854 mm, when the energy transmission coefficient is 0.016 and 0.051, respectively. This means that, although the phase-reversal condition is met, more than 94% of the incident energy will be reflected due to impedance mismatch between water and brass. This is the main reason why brass is usually employed to implement the pressure blocking regions of Soret FZPs. In contrast, if the lens is implemented in PLA, the π phase shift occurs at a thickness of 2.313 mm, when the squared transmission coefficient is higher than 97%. This fact makes PLA a suitable material for implementing PR-FZPs in underwater focusing applications, as its acoustic impedance is similar to the water impedance.
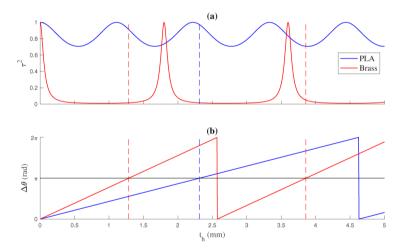
Figure 7.2: (a) Energy transmission coefficient as a function of the lens thickness and (b) phase difference between the host medium and the material. Blue lines correspond to PLA and red lines correspond to brass.

In order to demonstrate the improved acoustic focusing performance of 3D printed phase reversal lenses over conventional brass lenses, numerical simulations and experimental measurements have been carried out. Numerical simulations have been computed using COMSOL Multiphysics, which uses the

Table 7.1: Acoustic properties of water, PLA and brass.

	ρ (kg/m^3)	c (m/s)	Z (MRayl)	$|\Gamma|$
Water	1000	1500	1.5	N/A
PLA	1240	2220	2.753	0.17
Brass	8400	3600	30.24	0.99

Finite Element Method (FEM) to solve the wave equation in the different media. Experimental measurements have been developed using an automated 3D underwater positioning system. A needle hydrophone fixed to a programmable robotic arm is employed as receiver, while a directional piston transducer connected to a Pulser is employed as transmitter. The separation distance between lens and transducer is $d = 340$ mm, which is not enough to consider plane wave incidence and therefore the spherical wave design approach must be used. Additional details of the FEM model and the experimental set-up can be found at the **Methods** section.

Two different lenses have been manufactured, being one of them a conventional Soret FZP made of brass and the other a 3D printed PR-FZP made of PLA. Figure 7.3 shows both lenses, where Figure 7.3a corresponds to the FZP and Figure 7.3b corresponds to the PR-FZP. The PLA thickness is $t_h = 2.313$ mm, which provides the phase-reversal behaviour, as mentioned above. The brass thickness is $t_h = 0.5$ mm, which ensures a high reflection coefficient and therefore a good pressure blocking behaviour. For both lenses, the working frequency is 1 MHz, the focal distance is $F_L = 50$ mm and the number of Fresnel regions is $N = 16$, considering a source separation distance of $d = 340$ mm. As it can be observed from Figure 7.3 , both lenses have been manufactured with a central transparent zone instead of a central blocking/phase-reversal region. This design choice is selected as a consequence of the piston transducer, because with a central blocking region the main energy contribution of the transducer would be reflected, and with a phase-reversal region the energy transmission coefficient would be reduced.

Figure 7.4 shows acoustic intensity maps normalized to the global maximum, which is achieved in the PR-FZP case. Figure 7.4a and Figure 7.4b correspond to simulation results, while Figure 7.4c and Figure 7.4d correspond to experimental measurements. As it can be observed, numerical and experimental results agree very well, and the PLA PR-FZP lens (Figure 7.4b and
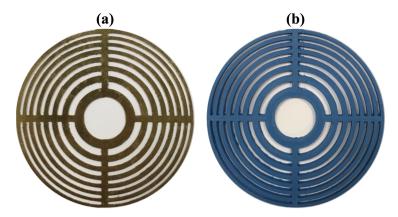
Figure 7.3: Manufactured lenses: (a) FZP made of brass and (b) PR-FZP made of PLA.

Figure 7.4d) achieves a higher focal intensity compared to the conventional brass FZP (Figure 7.4a and Figure 7.4c). The differences found between both lenses, in addition to those already mentioned above, are found in the size of the focus and the energy surrounding it. In the case of the conventional FZP, almost all the energy is concentrated in the focal area for both experimental and numerical results, while in the case of the PR-FZP the experimental measurements show that the focal area is increased compared with the numerical results. This fact is due to the effect of the cross-shape structural support of the PR-FZP, which is not included in the simulation model. This support introduces a π phase change at transparent Fresnel regions that generates a destructive interference at the focal distance, which increases the size of the focus in both longitudinal and radial directions, and therefore decreases the focusing efficiency of the lens. For the conventional FZP, the cross-shape structural support does not interfere destructively at the focal distance as the pressure is reflected at the brass, and therefore the focal area is not increased as in the PLA case.

Figure 7.5a and Figure 7.5b depict radial and longitudinal intensity cuts for both numerical and experimental results, respectively. Once again, the results are normalized to the maximum intensity value. An additional parameter to evaluate the focusing improvement factor of PR-FZPs over conventional FZPs can be defined as the ratio between the focal intensity of the PR-FZP and the focal intensity of the conventional FZP. Thus, as it can be seen in Figure 7.5a and Figure 7.5b, a considerable improvement factor of 220% is achieved when using the Phase-Reversal lens. Figure 7.5a also depicts an almost absence of
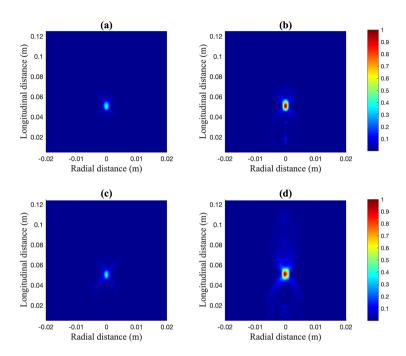
Figure 7.4: Measured intensity maps: FZP simulated (a) and measured (c), PR-FZP simulated (b) and measured (d).

secondary lobes for both lenses. This fact is due to the influence of the piston directional transducer, as its directivity pattern has an effect similar to the FZP apodization effect achieved through efficiency decreasing regions (Takeuchi, Uesugi, and Suzuki 2017), which reduces the secondary lobes. Focusing profiles of Figure 7.5b show that both lenses focus at the designed $F_L = 50$ mm focal distance, which means that the spherical wave incidence design approach works when using piston transducers.

One interesting parameter that can be used to characterize the focusing performance of a lens is the focusing efficiency. In this case, the focusing efficiency, η_F, is defined as the ratio between the energy at the focal area and the incident energy at the lens. The focal area is given by the focal radius, which is the radial distance which contains the main focusing lobe. Additional explanation of focusing efficiency calculations can be found in the **Methods** section. If an ideal model is considered, theoretical maximum focusing efficiencies of 12.2% and 42.1% are obtained for the conventional FZP and the PR-FZP, re-
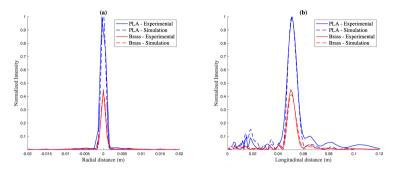
Figure 7.5: (a) Normalized radial intensity and (b) normalized longitudinal intensity for PR-FZP made of PLA (blue) and FZP made of brass (red). Solid lines correspond to experimental results, while dashed lines correspond to simulation results.

spectively. These values are indicators that, ideally, a PR-FZP could reach approximately four times the energy efficiency of a conventional FZP.

Table 7.2 shows a comparison between numerical and experimental results of the main focusing parameters of both lenses. The focal gain has been calculated as the ratio between the intensity achieved with the lens and the intensity measured in absence of the lens. As it can be observed, the manufactured PR-FZP achieves a focal gain of 21.9 dB, which results in an increase of 4.0 dB over the conventional FZP. The measured FLHM is 5.174λ for the FZP case and 5.87λ for the PR-FZP case, while the FWHM measured values are 0.87λ and 1.27λ for the FZP and PR-FZP case, respectively. This means that, as explained above, the focal area is increased in terms of both FLHM and FWHM when the PLA lens is employed instead of the brass lens. On the other hand, the focusing efficiency achieved with the PR-FZP is 30.20%, which results in more than twice the focusing efficiency achieved with the FZP (11.33%). If numerical and experimental results are compared, good agreement between FEM and measured parameters is observed. However, a slight difference between the FWHM value obtained from the FEM model and the experimental measurement can be found for the conventional FZP case. This phenomenon could be caused by the limitation in resolution of the experimental set-up. As explained in the **Methods** section, the experimental set-up has a spatial resolution of $1 \times 1 \times 1$ mm^3. At the working frequency of the lens (1 MHz), the host wavelength is $\lambda = 1.5$ mm, which is very close to the spatial resolution of the measurement system and therefore limits the accuracy of the measured FWHM values, which is approximately $FWHM \cong \lambda$.

Table 7.2: Simulated (FEM) and measured (Exp.) focusing characteristics of the FZP and PR-FZP.

	Gain (dB)	FLHM (λ)	FWHM (λ)	η_F (%)
FZP (FEM)	18.59	5.155	1.02	12.10
FZP (Exp.)	17.90	5.174	0.87	11.33
PR-FZP (FEM)	22.44	5.480	1.01	32.40
PR-FZP (Exp.)	21.90	5.870	1.27	30.20

7.4   Discussion

In this work, the design process and focusing properties of acoustic PR-FZP lenses have been analyzed. Simulation and experimental results are presented, and they show that 3D printed PR-FZPs made of PLA can achieve higher focusing efficiency and focal intensity gain than conventional Soret FZPs, with an improvement in both factors over 200%. The simulation results are experimentally validated, showing a good agreement between the FEM model and the measured intensity maps.

PR-FZPs implemented in PLA grant affordable acoustic lenses with high focusing efficiency. The 3D printing technology allows a reduction of the manufacturing costs compared to metal implemented lenses. In the medical field, acoustic lenses manufactured using 3D printing techniques result very useful due to their flexibility, since this type of lenses can be designed and built specifically for each treatment in a few hours. Moreover, these lenses could also be used in MRI environments due to its manufacturing material. PLA is a biocompatible material without electromagnetic interaction that has already been used in medical environments due to its structural qualities. Therefore, these PR-FZP lenses could be used in ultrasound focusing therapies with MRI real time monitoring with the characteristic of being able to be easily designed and manufactured *in situ*.

7.5 Methods

7.5.1 Focusing Efficiency

Diffraction is a phenomenon that occurs when an acoustic wave front impinges on an obstacle with an aperture or border. The acoustic intensity generated by a lens when the field is diffracted at its apertures can be calculated using the non-paraxial diffraction integral, which is given by:

$$I(z,r) = \frac{1}{\lambda^2} \left| \int_0^{2\pi} \int_0^{r_N} q(r')p_i(r')\frac{r'}{R}e^{-jkR}dr'd\varphi \right|^2 , \qquad (7.4)$$

Where $p_i(r')$ is the incident pressure at the lens, $q(r')$ is the pupil function of the lens, r' is the radial axis at the surface of the lens, r_N is the external radius of the lens, and $R = \sqrt{r^2 + (r')^2 + z^2 - 2rr'\cos\varphi}$, being φ the rotation angle at the surface of the lens. The pupil function describes the geometry of the lens. For an ideal Soret lens, the pupil function is 1 at transparent regions and 0 at pressure blocking regions, while for an ideal phase reversal lens the pupil function at phase reversal region is -1, which models the π phase shift.

As stated in **Results** section, the focusing efficiency can be defined as the ration between the energy at the focal area, W_F, and the incident energy at the lens, W_0. In this case, the focal area is defined as the region of the focal plane which contains the main focusing lobe, as depicted in Figure 7.6. Thus, the focusing efficiency can be calculated as

$$\eta_F = \frac{W_F}{W_0} = \frac{\int_0^{2\pi} \int_0^{r_F} I(z=F,r)rdrd\varphi}{\int_0^{2\pi} \int_0^{r_N} I_0(z=0,r)rdrd\varphi} = \frac{\int_0^{r_F} I(z=F,r)rdr}{\int_0^{r_N} I_0(z=0,r)rdr}, \qquad (7.5)$$

Where $I(z=F,r)$ represents the focal intensity, $I_0(z=0,r)$ represents the incident intensity, r_N is the outer radius of the lens and r_F is the focal radius.

When plane wave incidence is considered, the incident pressure can be expressed as $p_i = p_0 e^{jkz}$ and therefore the incident intensity is given by:

$$I_0(z=0,r) = \frac{|p_0|^2}{2Z_0} \qquad (7.6)$$
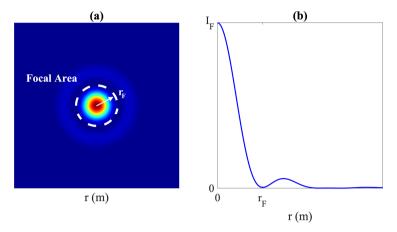
Figure 7.6: Scheme of the focusing efficiency calculation: (a) intensity at the focal plane and (b) radial intensity cut. The white dashed line marks the limit of the focal area.

Being p_0 the amplitude of the incident wave. With Equation (7.6), the incident energy can be directly calculated as:

$$W_0 = \int_0^{2\pi} \int_0^{r_N} I_0(z = 0, r) r \, dr \, d\varphi = \frac{|p_0|^2 \pi r_N^2}{2 Z_0} \qquad (7.7)$$

In contrast, when a directional piston transducer placed at a distance d from the lens is used as emitter, the incident pressure can be expressed as

$$p_i(r) = \frac{jk p_0 a^2}{2\sqrt{r^2 + d^2}} D(r) e^{-jk\sqrt{r^2 + d^2}} \qquad (7.8)$$

Where p_0 is the pressure at the surface of the piston, a is the piston active radius and $D(r)$ is the piston directivity pattern, which is given by:

$$D(r) = \frac{2 J_1(kar/\sqrt{r^2 + d^2})}{kar/\sqrt{r^2 + d^2}}, \qquad (7.9)$$

Being J_1 the first kind and first order Bessel function.

Therefore, for the piston transducer case the incident energy can be calculated by numerically the following expression:

$$W_0 = \frac{|p_0|^2 \pi a^2}{Z_0} \int_0^{r_N} \frac{1}{r} J_1 \left(ka \frac{r}{\sqrt{r^2 + d^2}} \right)^2 dr. \tag{7.10}$$

The focal intensity generated by the lens can be calculated by numerically computing Equation (7.4). Once the focal intensity is obtained, the energy at the focus, W_F, can be computed by integrating the result over the focal area. Subsequently, the focusing efficiency can be calculated using Equation (7.7) and Equation (7.10) for the plane wave and piston transducer case, respectively. Table Table 7.3 shows a comparison between the focusing efficiency values of an ideal FZP and an ideal PR-FZP with $N = 16$ regions and $F = 50$ mm. The ideal FZP implements perfect pressure blocking regions with $|\Gamma| = 1$, while the ideal PR-FZP implements perfect phase-reversal regions with $|\Gamma| = 0$. Both lenses have a transparent central region and a working frequency of 1 MHz. For the piston transducer case, a separation of $d = 340$ mm between lens and emitter and an active radius of $a = 6.35$ mm have been considered. As it can be observed from the results shown in Table 7.3, the PR-FZP achieves higher focusing efficiency than the conventional FZP in both the plane wave incidence case and the piston transducer case. Moreover, it is worth noting that in the piston transducer case both FZPs reach higher efficiency values compared to the plane wave case. This fact can be explained by the directional behaviour of the piston transducer, which concentrates the main energy contributions on the central regions of the lens.

Table 7.3: Focusing efficiency (η_F) comparison between plane wave and piston transducer case.

	Plane wave (%)	Piston transducer (%)
FZP	9.9	12.2
PR-FZP	37.0	42.1

The experimental value of the focusing efficiency can be obtained by carrying out two different measurement steps. The first step is performed with the lens, and it consists of the measurement of the radial intensity at the focal plane, that is, $I(z = F, r)$. The second step is performed without the lens, and it consists of the measurement of the incident intensity at the lens, $I_0(z = 0, r)$.

In this measurement, the radial intensity is measured at the position where the lens was placed at the first step. Finally, the focusing efficiency can be calculated by numerically computing Equation (7.5).

The experimental value of the focusing efficiency can be obtained by carrying out two different measurement steps. The first step is performed with the lens, and it consists of the measurement of the radial intensity at the focal plane, that is, $I(z = F, r)$. The second step is performed without the lens, and it consists of the measurement of the incident intensity at the lens, $I_0(z = 0, r)$. In this measurement, the radial intensity is measured at the position where the lens was placed at the first step. Finally, the focusing efficiency can be calculated by numerically computing Equation (7.5).

7.5.2 FEM model explanation

The numerical model is shown in Figure 7.7 and it can be observed that only a half-plane of the lens has been considered to take advantage of the axisymmetric condition. This approach reduces the number of degrees of freedom and therefore the computational burden of the problem. The piston transducer has been modeled as a pressure condition of 1 Pa placed at a distance $d = 340$ mm from the lens. In order to avoid reflections, a radiation condition has been set at the outer boundaries in order to emulate the Sommerfeld condition. The acoustic properties of the different materials considered can be found in Table 7.1 of **Results** section.
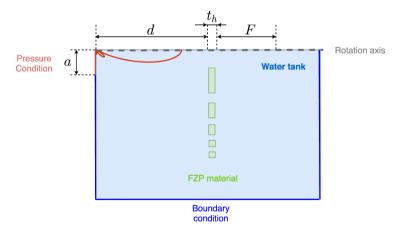
Figure 7.7: Scheme of the geometry and boundary conditions of the Finite Element Method model.

The study of the physical phenomena involved in the interaction between the lenses and the wave front requires a mathematical model that considers the boundary conditions of the problem. In the present work, the commercial software COMSOL Multiphysics (Multiphysics 2012), which implements the FEM method, has been used to calculate the acoustic pressure distribution generated by the lens. This method obtains a numerical solution by discretizing the model depicted in Figure 7.7 and solving the Helmholtz Partial Differential Equation:

$$\nabla \cdot \left(-\frac{1}{\rho}(\nabla p) \right) = \frac{k^2 p}{\rho}. \tag{7.11}$$

7.5.3   Experimental set-up description

In order to validate numerical results, experimental measures have been carried out. To perform the experimental measurements, a high-precision underwater measurement system of the Centro de Tecnologías Físicas (Universitat Politècnica de València) has been used. The measurement robot is installed in an immersion tank filled of distilled water, which dimensions are $0.5 \times 0.5 \times 1$ m^3. This system consists of a fixed emitter and a receiver coupled to programmable robotic arms, which can measure with a spatial resolution of $1 \times 1 \times 1$ mm^3. A plane immersion piston transducer built by Olympus with 1 MHz of central working frequency and an active diameter of 12.7 mm has been used as emitter and a Precision Acoustics needle hydrophone is used as receiver. The transmitted signal is generated using a Panametrics Pulser, while the received signal is digitized using a Digital Oscilloscope from Pico Technology. The measurement process is automated and controlled using a LabView program installed on a PC. Figure 7.8 shows the experimental set-up in a measurement.
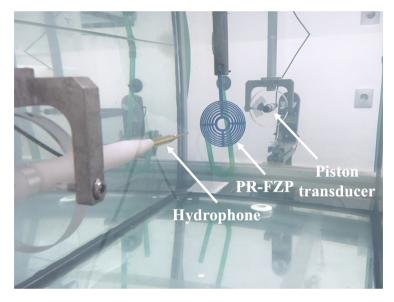
Figure 7.8: Experimental set-up.

Chapter 8

Discussion

The overall objective (General Objective 1) was to improve tumor resolution capacity with HIFU transducers for tumor ablation. The idea was to implement acoustic lenses based on subwavelength structures (General Objective 1.1) that allow the characteristics of the focal area to be controlled. Therefore, the main parameters with which these improvements in resolution can be achieved were studied (Specific Objective 1). The characteristics to improve are the depth of focus (DoF) and the lateral resolution (R_{lat}) that are linked to the FWHM and the FLHM. All the proposals developed throughout this thesis have started from numerical models that have been analyzed using the finite element method (FEM) as specified (Specific Objective 2). FEM models are created that accurately reproduce the diffractive processes to which an acoustic field is subjected as it passes through sub-wavelength structures. These models are experimentally validated in controlled situations (Specific Objective 3). The lenses that have been developed and analyzed in this thesis comply with the hypotheses proposed, that is, that they are capable of reducing the time of exposure of a patient to HIFU therapy, improving the gain (General Objective 2) and achieving better longitudinal and axial resolution, therefore improving energy distribution (General Objective 2.1). That said, we can encompass the objectives in 3 blocks: Improving gain, improving the resolution and compatibility with MRI systems. First, a Fresnel lens (FZP) was selected as the starting system. The characteristic of this lens typology, as mentioned,

is its high focusing capacity, its flat geometry and the ease of implementation in different systems. From this moment, improvements have been applied to a 19th century design, transferring concepts of optics and electromagnetism and relying on the knowledge acquired in the study of acoustics.

One of the first improvements was made by modifying the classical construction equation and introducing the reference radius / phase concept. This study was published in the first article of the doctoral thesis entitled "Manipulation of focal patterns in acoustic Soret type zone plate lens by using reference radius / phase effect". Through this modification, two phenomena were found based on the values of r_1 and r_0. In the event that r_1 was less than r_0 there was an improvement in the SLL. This phenomenon is due to the control of the constructive interferences of the diffracted waves from the circular zones. By changing the size of the reference radius, the spatial frequency of the FZP changes as well. This phenomenon allows the creation of a much finer focus, therefore improving lateral resolution. At this point, we realized that choosing a reference radius r_1 greater than r_0 causes another effect related to apodization. When this occurs, it can be affirmed that the effect occurs in the same way as if we introduced a pupil mask, leading us to carry out two pieces of work that would end in two articles.

The articles "Design of Acoustical Bessel-Like Beam Formation by a Pupil Masked Soret Zone Plate Lens" and "Tunable depth of focus of acoustical pupil masked Soret Zone Plate" focus on the study of the effect of the pupil mask. The first of these focuses on the design, using the pupil mask, of a quasi-non-diffracting transverse sub-wavelength beam. What is happening on a physical level is the conversion of the converging spherical waves into quasi-conical waves. This generates an improvement in spatial resolution of 21% and a beam length expansion of 209% compared to a classic FZP lens. In the second article, a comprehensive study of the effect of the pupil mask is performed. The size of the DoF is related to both the size of the pupil mask and the diameter of the lens and its numerical aperture. Therefore, very extended foci (which implies a very high DoF) can be achieved due to the circular grids that generate the quasi-Bessel beam. In summary, the application of the pupil mask leads to a compromise between lateral resolution and beam length.

Once the objective of improving the resolution, that is, being able to modify the R_{lat} and the DoF of a lens, was covered, it was pending that it could be used in MRI environments. The key was to be able to implement a lens using materials that had no electromagnetic interaction. In previous works, brass had been used as a material with ease of machining, high contrast of impedances with water, and therefore, to make the first approximation models, it was an

excellent material. One of the needs in HIFU applications is the fact that the guidance is through MRI. In the article "MRI Compatible Planar Material Acoustic Lenses" 3 materials that do not have electromagnetic interaction are compared: Polymethylmethacrylate (PMMA), acrylonitrile butadiene styrene (ABS) and polylactic acid (PLA). It is shown that for the Soret condition to be fulfilled in the implementation of a FZP, the impairment contrast must be the highest possible. In this case, the use of a lens constructed with PLA is proposed, the rings of which have an air chamber. It is concluded that PLA is one of the ideal materials for the construction of compatible MRI lenses and that it is possible to build lenses that meet this condition. The possibility of implementing lenses through 3D printing opens the door to new possibilities, with PLA being a relatively cheap and biocompatible material (unlike PMMA). In any case, it happens that over time, PLA degrades and can form micropores on the surface. In the end, this will cause the water to gradually enter the lens reducing the contrast and therefore reducing the efficiency of the lens. At this point, the last paper that brings the thesis to a climax is proposed.

So far, using an FZP distribution, it has been possible to improve its resolution properties and add a control of DoF and R_{lat} using a pupil mask. Furthermore, it has been possible to build an FZP in materials that are MRI compatible. These enhancements have been implemented using a Soret-based construction of the FZP, that is, the rings block destructive contributions to focus. To achieve the objective of improving the gain, the hypothesis of achieving that all the rings contribute constructively to the focal conformation is proposed. For this reason, a lens made entirely of PLA is modeled, thereby removing the need for air chambers to achieve the impedance contrast. In the article "Acoustic Focusing Enhancement in Fresnel Zone Plate Lenses" it is possible to build a lens based on the phase inversion of an FZP that improves efficiency and gain by 200% compared to a traditional FZP. With all this, it is proposed that the lenses to be used in HIFU treatments can be implemented in a few hours or even minutes depending on the capabilities of the 3D printer *ad-hoc*.

Chapter 9

Conclusions

1. It is possible to increase the spatial resolution in ultrasound transducers for HIFU purposes. Thus, acoustic lenses based on subwavelength structures were developed and implemented. The use of pupil-masks in FZP improve focal zone energy control.

2. Improving the focusing capacity will result into HIFU treatments exposure time for future implementations.

3. The new Phase-Reversal FZP typology allows extraordinary transmission that improves focal gain in 3 dimensions by up to more than 200% compared to a Soret FZP.

4. Acoustic lenses improve HIFU transducer parameters as R_{lat}, DoF and gain. In addition, construction of acoustic lenses using non-metallic materials is possible. Therefore, it is possible to build lenses using biocompatible materials. The fact of using materials that can be used by 3D printers will allow acoustic lenses *ad hoc* implementation.

5. FEM-based models have been developed that have been validated through experiments. Therefore, it is possible to predict the behavior of an acoustic lens by replicating the behavior of the physics involved.

Bibliography

Albu, S. et al. (2004). "Potential for the use of ultrasound in the extraction of antioxidants from Rosmarinus officinalis for the food and pharmaceutical industry". In: *Ultrasonics Sonochemistry* 10.3, pp. 261–265. ISSN: 13504177. DOI: `10.1016/j.ultsonch.2004.01.015` (cit. on pp. 14, 26, 50).

Amemiya, Isao et al. (1997). "Ink jet printing with focused ultrasonic beams". In: *Proc. NIP 13: International Conference on Digital Printing Technologies* 5, pp. 274–279 (cit. on pp. 14, 15, 26, 40).

Aubry, Jean-Francois et al. (2013). "The road to clinical use of high-intensity focused ultrasound for liver cancer: technical and clinical consensus". In: *Journal of Therapeutic Ultrasound* 1.1, p. 13. ISSN: 2050-5736. DOI: `10.1186/2050-5736-1-13` (cit. on p. 15).

Babinet, Jacques (1837). *Memoires d'optique méteorologique* (cit. on p. 41).

Bashford, A. G. et al. (1997). "Field characterization of an air-coupled micromachined ultrasonic capacitance transducer". In: *The Journal of the Acoustical Society of America* 101.1, pp. 315–322. ISSN: 0001-4966. DOI: `10.1121/1.418011` (cit. on pp. 15, 27).

Black, D.N. and J.C. Wiltse (1987). "Millimeter-Wave Characteristics of Phase-Correcting Fresnel Zone Plates". In: *IEEE Transactions on Microwave*

Theory and Techniques 35.12, pp. 1122–1129. ISSN: 0018-9480. DOI: `10.1109/TMTT.1987.1133826` (cit. on p. 64).

Born, Max and Emil Wolf (2013). *Principles of optics: electromagnetic theory of propagation, interference and diffraction of light*. Elsevier. ISBN: 148310320X (cit. on pp. 27, 32).

Bragg, W. H. and Bragg W. L. (1913). "The reflection of X-rays by crystals". In: *Proceedings of the Royal Society of London. Series A, Containing Papers of a Mathematical and Physical Character* 88.605, pp. 428–438. ISSN: 0950-1207. DOI: `10.1098/rspa.1913.0040` (cit. on p. 43).

Burckhardt, C. B., H. Hoffmann, and P.-A. Grandchamp (1973). "Ultrasound Axicon: a device for focusing over a large depth". In: *The Journal of the Acoustical Society of America* 54.6, pp. 1628–1630. ISSN: 0001-4966. DOI: `10.1121/1.1914459` (cit. on p. 41).

Calvo, D. C. et al. (2015a). "Thin Fresnel zone plate lenses for focusing underwater sound". In: *Applied Physics Letters* 107.1, p. 014103. ISSN: 0003-6951. DOI: `10.1063/1.4926607` (cit. on pp. 15, 27, 29, 40, 50, 63, 65).

Calvo, David C. et al. (2015b). "Thin Fresnel zone plate lenses for underwater acoustics: Modeling and experiments". In: *OCEANS 2015 - MTS/IEEE Washington*. IEEE, pp. 1–6. ISBN: 978-0-9339-5743-5. DOI: `10.23919/OCEANS.2015.7401947` (cit. on pp. 14, 26, 40).

Castiñeira-Ibáñez, S. et al. (2016). "An Ultrasonic Lens Design Based on Prefractal Structures". In: *Symmetry* 8.4, p. 28. ISSN: 2073-8994. DOI: `10.3390/sym8040028` (cit. on pp. 40, 55).

Castiñeira-Ibáñez, S. et al. (2018). "Polyadic Cantor Fractal Ultrasonic Lenses: Design and Characterization". In: *Applied Sciences* 8.8, p. 1389. ISSN: 2076-3417. DOI: `10.3390/app8081389` (cit. on p. 50).

Castiñeira-Ibáñez, S. et al. (2019). "Tunable depth of focus of acoustical pupil masked Soret Zone Plate". In: *Sensors and Actuators A: Physical* 286, pp. 183–187. ISSN: 09244247. DOI: `10.1016/j.sna.2018.11.053` (cit. on p. 63).

Cervera, F. et al. (2001). "Refractive Acoustic Devices for Airborne Sound". In: *Physical Review Letters* 88.2, p. 023902. ISSN: 0031-9007. DOI: `10.1103/PhysRevLett.88.023902` (cit. on pp. 14, 26, 50, 62).

Chan, Shiu C. et al. (1995). "Finite Element Modeling of Binary Acoustic Fresnel Lenses". In: *Review of Progress in Quantitative Nondestructive Evaluation*. Boston, MA: Springer US, pp. 923–930. DOI: `10.1007/978-1-4615-1987-4_116` (cit. on p. 15).

Chen, Dong, Sanjay K. Sharma, and Ackmez Mudhoo (2011). *Handbook on Applications of Ultrasound*. Ed. by Dong Chen, Sanjay K. Sharma, and Ackmez Mudhoo. CRC Press, p. 739. ISBN: 9780429105746. DOI: `10.1201/b11012` (cit. on p. 62).

Clement, G., H. Nomura, and T. Kamakura (2015). "Ultrasound field measurement using a binary lens". In: *IEEE Transactions on Ultrasonics, Ferroelectrics, and Frequency Control* 62.2, pp. 350–359. ISSN: 0885-3010. DOI: `10.1109/TUFFC.2014.006800` (cit. on pp. 14, 29).

Cruz, J. J. (2013). "XIV Congreso Nacional en Salamanca de la Sociedad Española de Oncología Médica". In: *SEOM* (cit. on p. 1).

Doroshow, J. H. (2016). "Approach to the patient with cancer". In: *Goldman-Cecil Medicine. 26th ed. Philadelphia, PA: Elsevier Saunders* (cit. on p. 2).

Drumright, R. E., P. R. Gruber, and D. E. Henton (2000). "Polylactic Acid Technology". In: *Advanced Materials* 12.23, pp. 1841–1846. ISSN: 0935-9648. DOI: `10.1002/1521-4095(200012)12:23<1841::AID-ADMA1841>3.0.CO;2-E` (cit. on pp. 51, 64).

Dyson, James (1958). "Circular and spiral diffraction gratings". In: *Proceedings of the Royal Society of London. Series A. Mathematical and Physical Sciences* 248.1252, pp. 93–106. ISSN: 0080-4630. DOI: `10.1098/rspa.1958.0231` (cit. on pp. 41, 43).

Ebbini, E.S. and C.A. Cain (1991). "A spherical-section ultrasound phased array applicator for deep localized hyperthermia". In: *IEEE Transactions on Biomedical Engineering* 38.7, pp. 634–643. ISSN: 00189294. DOI: `10.1109/10.83562` (cit. on p. 64).

Escoffre, Jean-Michel and Ayache Bouakaz (2015). *Therapeutic ultrasound.* Vol. 880. Springer. ISBN: 3319225367 (cit. on p. 15).

Estrada, Héctor et al. (2008). "Extraordinary sound screening in perforated plates". In: *Physical review letters* 101.8, p. 084302 (cit. on p. 4).

Estrada, Héctor et al. (2009). "Angle-dependent ultrasonic transmission through plates with subwavelength hole arrays". In: *Physical review letters* 102.14, p. 144301 (cit. on p. 4).

Farnow, S. A. and B. A. Auld (1974). "Acoustic Fresnel zone plate transducers". In: *Applied Physics Letters* 25.12, pp. 681–682. ISSN: 0003-6951. DOI: 10.1063/1.1655359 (cit. on pp. 27, 40).

Fetting, John et al. (1996). "Outcomes of cancer treatment for technology assessment and cancer treatment guidelines". In: *Journal of Clinical Oncology* 14.2, pp. 671–679 (cit. on p. 2).

Fresnel, Augustin-Jean (1996). "Calcul de l'intensite de la lumiere au centre de l'ombre d'un ecran et d'une ouverture circulaires eclairepar un point radieux". In: *SPIE MILESTONE SERIES MS* 128, pp. 3–10 (cit. on p. 40).

Fuster, José et al. (2017). "Analysis of Fresnel Zone Plates Focusing Dependence on Operating Frequency". In: *Sensors* 17.12, p. 2809. ISSN: 1424-8220. DOI: 10.3390/s17122809 (cit. on pp. 29, 64).

Goh, Chiew Loon et al. (2018). "Sensing wood decay in standing trees: A review". In: *Sensors and Actuators A: Physical* 269, pp. 276–282. ISSN: 09244247. DOI: 10.1016/j.sna.2017.11.038 (cit. on p. 40).

Gomez-Lozano, Vicente et al. (2014). "Ultrasonic lens based on a subwavelength slit surrounded by grooves". In: *Sensors* 14.5, pp. 8821–8828 (cit. on p. 4).

Guenneau, Sébastien et al. (2007). "Acoustic metamaterials for sound focusing and confinement". In: *New Journal of Physics.* ISSN: 13672630. DOI: 10.1088/1367-2630/9/11/399 (cit. on pp. 14, 26).

Herrmann, Karl-Heinz et al. (2014). "3D printing of MRI compatible components: Why every MRI research group should have a low-budget 3D printer". In: *Medical Engineering & Physics* 36.10, pp. 1373–1380. ISSN: 13504533. DOI: `10.1016/j.medengphy.2014.06.008` (cit. on pp. 51, 63).

Hon, S. F. et al. (2010). "Self-focused acoustic ejectors for viscous liquids". In: *Review of Scientific Instruments* 81.6, p. 065102. ISSN: 0034-6748. DOI: `10.1063/1.3442526` (cit. on pp. 14, 26, 40).

Hsu, D. K., F. J. Margetan, and D. O. Thompson (1989). "Bessel beam ultrasonic transducer: Fabrication method and experimental results". In: *Applied Physics Letters* 55.20, pp. 2066–2068. ISSN: 0003-6951. DOI: `10.1063/1.102107` (cit. on pp. 28, 41).

Huder, B. and W. Menzel (1988). "Flat printed reflector antenna for mm-wave applications". In: *Electronics Letters* 24.6, p. 318. ISSN: 00135194. DOI: `10.1049/el:19880214` (cit. on p. 64).

Hyun, Jaeyub et al. (2018). "Realization of an ultrathin acoustic lens for sub-wavelength focusing in the megasonic range". In: *Scientific Reports* 8.1, p. 9131. ISSN: 2045-2322. DOI: `10.1038/s41598-018-27312-5` (cit. on p. 26).

IARC, International Agency for Research on Cancer (2020). "Cancer Incidence in Five Continents". In: *Online repository accessed August 2020: `http://ci5.iarc.fr`* (cit. on p. 1).

Illing, R O et al. (2005). "The safety and feasibility of extracorporeal high-intensity focused ultrasound (HIFU) for the treatment of liver and kidney tumours in a Western population". In: *British Journal of Cancer* 93.8, pp. 890–895. ISSN: 0007-0920. DOI: `10.1038/sj.bjc.6602803` (cit. on pp. 14, 26).

Institute, National Cancer (2019). "Types of cancer treatment". In: *Online repository accessed August 2020: `www.cancer.gov/about-cancer/treatment/types`* (cit. on p. 2).

Jang, Jihun and Jin Chang (2016). "Design and Fabrication of Double-Focused Ultrasound Transducers to Achieve Tight Focusing". In: *Sensors* 16.8, p. 1248. ISSN: 1424-8220. DOI: `10.3390/s16081248` (cit. on p. 26).

Jian-Yu Lu and J.F. Greenleaf (1994). "A study of two-dimensional array transducers for limited diffraction beams". In: *IEEE Transactions on Ultrasonics, Ferroelectrics and Frequency Control* 41.5, pp. 724–739. ISSN: 0885-3010. DOI: 10.1109/58.308509 (cit. on pp. 28, 41).

Jiménez, N. et al. (2014). "Acoustic Bessel-like beam formation by an axisymmetric grating". In: *EPL (Europhysics Letters)* 106.2, p. 24005. ISSN: 0295-5075. DOI: 10.1209/0295-5075/106/24005 (cit. on pp. 28, 41).

Kalosha, V. P. and I. Golub (2007). "Toward the subdiffraction focusing limit of optical superresolution". In: *Optics Letters* 32.24, pp. 3540–3542. ISSN: 0146-9592. DOI: 10.1364/OL.32.003540 (cit. on p. 41).

Kanevsky, I N (1977). *Focusing of Sound and Ultrasound Waves* (cit. on pp. 15, 27).

Karim-Kos, Henrike E et al. (2008). "Recent trends of cancer in Europe: a combined approach of incidence, survival and mortality for 17 cancer sites since the 1990s". In: *European journal of cancer* 44.10, pp. 1345–1389 (cit. on p. 1).

Katchadjian, P. et al. (2010). "APPLICATION OF AXICON LENSES IN ULTRASONIC TECHNIQUES". In: pp. 1043–1050. DOI: 10.1063/1.3362147 (cit. on pp. 28, 41).

Kennedy, James E (2005). "High-intensity focused ultrasound in the treatment of solid tumours". In: *Nature reviews cancer* 5.4, pp. 321–327 (cit. on p. 3).

Kennedy, James E, GR Ter Haar, and D Cranston (2003). "High intensity focused ultrasound: surgery of the future?" In: *The British journal of radiology* 76.909, pp. 590–599 (cit. on p. 3).

Kinsler, Lawrence E et al. (1999). *Fundamentals of Acoustics 4th Edition.* 4th Editio. Wiley-VCH, p. 560. ISBN: 0-471-84789-5 (cit. on p. 52).

Köhler, Max O. et al. (2009). "Volumetric HIFU ablation under 3D guidance of rapid MRI thermometry". In: *Medical Physics* 36.8, pp. 3521–3535. ISSN: 00942405. DOI: 10.1118/1.3152112 (cit. on p. 51).

Kundu, T et al. (2010). "Ultrasonic field modeling: a comparison of analytical, semi-analytical, and numerical techniques". In: *IEEE Transactions on Ultrasonics, Ferroelectrics and Frequency Control* 57.12, pp. 2795–2807. ISSN: 0885-3010. DOI: `10.1109/TUFFC.2010.1753` (cit. on p. 65).

Li, Ji-Tai et al. (2003). "An efficient synthesis of 3,4-dihydropyrimidin-2-ones catalyzed by NH2SO3H under ultrasound irradiation". In: *Ultrasonics Sonochemistry* 10.3, pp. 119–122. ISSN: 13504177. DOI: `10.1016/S1350-4177(03)00092-0` (cit. on pp. 14, 26, 50).

Li, Yajun and Emil Wolf (1981). "Focal shifts in diffracted converging spherical waves". In: *Optics Communications* 39.4, pp. 211–215. ISSN: 00304018. DOI: `10.1016/0030-4018(81)90108-5` (cit. on p. 20).

Li, Yong et al. (2012). "Acoustic focusing by coiling up space". In: *Applied Physics Letters* 101.23, p. 233508. ISSN: 0003-6951. DOI: `10.1063/1.4769984` (cit. on pp. 14, 26, 50).

Li, Yong et al. (2015). "Three-dimensional Ultrathin Planar Lenses by Acoustic Metamaterials". In: *Scientific Reports* 4.1, p. 6830. ISSN: 2045-2322. DOI: `10.1038/srep06830` (cit. on p. 63).

Lin, Zhou et al. (2014). "Acoustic focusing of sub-wavelength scale achieved by multiple Fabry-Perot resonance effect". In: *Journal of Applied Physics* 115.10, p. 104504. ISSN: 0021-8979. DOI: `10.1063/1.4868629` (cit. on p. 62).

Machado, Federico et al. (2018). "Terahertz Sieves". In: *IEEE Transactions on Terahertz Science and Technology* 8.1, pp. 140–143. ISSN: 2156-342X. DOI: `10.1109/TTHZ.2017.2762292` (cit. on p. 64).

Marsac, L. et al. (2012). "MR-guided adaptive focusing of therapeutic ultrasound beams in the human head". In: *Medical Physics* 39.2, pp. 1141–1149. ISSN: 00942405. DOI: `10.1118/1.3678988` (cit. on p. 63).

Masuyama, Hiroyuki and Koichi Mizutani (2006). "Acoustic Beam Scanning Using Annular Transducer Array Introducing Decentering Operation". In: *JSME International Journal Series C* 49.3, pp. 681–686. ISSN: 1347-538X. DOI: `10.1299/jsmec.49.681` (cit. on p. 28).

Masuyama, Hiroyuki et al. (1999). "Generation of Bessel Beam from Equiamplitude-Driven Annular Transducer Array Consisting of a Few Elements". In: *Japanese Journal of Applied Physics* 38.Part 1, No. 5B, pp. 3080–3084. ISSN: 0021-4922. DOI: 10.1143/JJAP.38.3080 (cit. on pp. 28, 41).

McCann, D.M and M.C Forde (2001). "Review of NDT methods in the assessment of concrete and masonry structures". In: *NDT & E International* 34.2, pp. 71–84. ISSN: 09638695. DOI: 10.1016/S0963-8695(00)00032-3 (cit. on pp. 14, 26, 50).

McDannold, Nathan et al. (1998). "MRI evaluation of thermal ablation of tumors with focused ultrasound". In: *Journal of Magnetic Resonance Imaging* 8.1, pp. 91–100. ISSN: 10531807. DOI: 10.1002/jmri.1880080119 (cit. on p. 51).

McGloin, D and K Dholakia (2005). "Bessel beams: Diffraction in a new light". In: *Contemporary Physics* 46.1, pp. 15–28. ISSN: 0010-7514. DOI: 10.1080/0010751042000275259 (cit. on p. 28).

Minin, I. V. and O. V. Minin (1990). "Control of focusing properties of diffraction elements". In: *Soviet Journal of Quantum Electronics* 20.2, pp. 198–199. ISSN: 0049-1748. DOI: 10.1070/QE1990v020n02ABEH005584 (cit. on pp. 15, 16, 28, 29).

Minin, I V and O V Minin (2004). *Diffractional optics of millimetre waves.* London: IOP Publishing. ISBN: 1420034480 (cit. on p. 27).

Minin, I. V. and O. V. Minin (2008). *Basic principles of Fresnel antenna arrays.* Vol. 19. Springer Science & Business Media. ISBN: 3540795596 (cit. on pp. 15, 27).

Minin, I. V. and O. V. Minin (2011a). "3D High-Quality Ultrasonic Imaging". In: *Ultrasound Imaging - Medical Applications.* InTech. DOI: 10.5772/16460 (cit. on pp. 40, 62).

Minin, I V et al. (2007). "Investigation of the resolution of phase correcting Fresnel lenses with small focal length-to-diameter ratio and subwavelength focus". In: *Proceeding of the EMTS 2007*, pp. 26–28 (cit. on p. 27).

Minin, Igor V. and O. V. Minin (2011b). "Reference Phase in Diffractive Lens Antennas: A Review". In: *Journal of Infrared, Millimeter, and Terahertz Waves* 32.6, pp. 801–822. ISSN: 1866-6892. DOI: 10.1007/s10762-011-9786-5 (cit. on pp. 15, 16, 29, 30).

Molerón, Miguel, Marc Serra-Garcia, and Chiara Daraio (2014). "Acoustic Fresnel lenses with extraordinary transmission". In: *Applied Physics Letters* 105.11, p. 114109 (cit. on p. 4).

Molerón, Miguel, Marc Serra-Garcia, and Chiara Daraio (2014). "Acoustic Fresnel lenses with extraordinary transmission". In: *Applied Physics Letters* 105.11, p. 114109. ISSN: 0003-6951. DOI: 10.1063/1.4896276 (cit. on pp. 14, 26, 40, 63).

Multiphysics, COMSOL (2012). "Comsol multiphysics user guide (version 4.3 a)". In: *COMSOL, AB*, pp. 39–40 (cit. on pp. 17, 30, 43, 51, 77).

Nagai, S. and K. Iizuka (1982). "A practical ultrasound axicon for non-destructive testing". In: *Ultrasonics* 20.6, pp. 265–270. ISSN: 0041624X. DOI: 10.1016/0041-624X(82)90047-6 (cit. on p. 41).

O'Shea, Donald C et al. (2004). *Diffractive optics: design, fabrication, and test.* Vol. 62. SPIE press. ISBN: 0819451711 (cit. on pp. 14, 27).

Park, Jong Ju et al. (2009). "Table-top soft x-ray microscope adopting a PMMA phase-reversal zone plate". In: *Conference on Lasers and Electro-Optics/International Quantum Electronics Conference.* Washington, D.C.: OSA, JFA6. ISBN: 978-1-55752-869-8. DOI: 10.1364/CLEO.2009.JFA6 (cit. on p. 63).

Peng, Pai, Bingmu Xiao, and Ying Wu (2014). "Flat acoustic lens by acoustic grating with curled slits". In: *Physics Letters A* 378.45, pp. 3389–3392. ISSN: 03759601. DOI: 10.1016/j.physleta.2014.09.042 (cit. on pp. 14, 26, 50, 62).

Pérez-López, Sergio et al. (2018). "On the use of phase correction rings on Fresnel zone plates with ultrasound piston emitters". In: *Applied Physics Letters* 112.26, p. 264102. ISSN: 0003-6951. DOI: 10.1063/1.5036712 (cit. on pp. 41, 65).

Pignoli, P et al. (1986). "Intimal plus medial thickness of the arterial wall: a direct measurement with ultrasound imaging." In: *Circulation* 74.6, pp. 1399–1406. ISSN: 0009-7322. DOI: 10.1161/01.CIR.74.6.1399 (cit. on p. 26).

Qin, Fei et al. (2015). "Shaping a Subwavelength Needle with Ultra-long Focal Length by Focusing Azimuthally Polarized Light". In: *Scientific Reports* 5.1, p. 9977. ISSN: 2045-2322. DOI: 10.1038/srep09977 (cit. on pp. 34, 45).

Rayleigh, John William Strutt Baron (1888). *Wave Theory, vol 24.* Encyclopedia Britannica (cit. on p. 64).

— (1899). *Scientific papers.* Vol. 1. University Press (cit. on p. 40).

REDECAN (2020). "Red Española de Registros de Cáncer". In: *Online repository accessed August 2020: http: // redecan. es/ redecan. org/ es/ page3f38. html? id= 218 title= estadisticas* (cit. on p. 1).

Rocca-Smith, Jeancarlo R. et al. (2017). "Beyond Biodegradability of Poly(lactic acid): Physical and Chemical Stability in Humid Environments". In: *ACS Sustainable Chemistry & Engineering* 5.3, pp. 2751–2762. ISSN: 2168-0485. DOI: 10.1021/acssuschemeng.6b03088 (cit. on p. 51).

Roy, Tapashree et al. (2014). "Point spread function of the optical needle superoscillatory lens". In: *Applied Physics Letters* 104.23, p. 231109. ISSN: 0003-6951. DOI: 10.1063/1.4882246 (cit. on pp. 34, 45).

Rubio, Constanza et al. (2017). "Pinhole Zone Plate Lens for Ultrasound Focusing". In: *Sensors* 17.7, p. 1690. ISSN: 1424-8220. DOI: 10.3390/s17071690 (cit. on pp. 35, 44).

Schindel, D.W., A.G. Bashford, and D.A. Hutchins (1997). "Focussing of ultrasonic waves in air using a micromachined Fresnel zone-plate". In: *Ultrasonics* 35.4, pp. 275–285. ISSN: 0041624X. DOI: 10.1016/S0041-624X(97) 00011-5 (cit. on p. 63).

Schonbrun, Ethan, Charles Rinzler, and Kenneth B. Crozier (2008). "Microfabricated water immersion zone plate optical tweezer". In: *Applied Physics*

Letters 92.7, p. 071112. ISSN: 0003-6951. DOI: `10.1063/1.2837538` (cit. on pp. 14, 26, 40).

Shimizu, Hiroshi, N Chubachi, and J I Kushibiki (1989). "Acoustical Imaging". In: *Plenum Press, New York and London* 17 (cit. on pp. 15, 27).

Soret, J. L. (1875). "Ueber die durch Kreisgitter erzeugten Diffractionsphänomene". In: *Annalen der Physik und Chemie* 232.9, pp. 99–113. ISSN: 00033804. DOI: `10.1002/andp.18752320906` (cit. on pp. 14, 27, 29, 40, 50, 63).

Stratton, Julius Adams (2007). *Electromagnetic theory*. Vol. 33. John Wiley & Sons. ISBN: 0470131535 (cit. on p. 41).

Takeuchi, A, K Uesugi, and Y Suzuki (2017). "Improvement of quantitative performance of imaging x-ray microscope by reduction of edge-enhancement effect". In: *Journal of Physics: Conference Series* 849, p. 012055. ISSN: 1742-6588. DOI: `10.1088/1742-6596/849/1/012055` (cit. on p. 70).

Tarrazó-Serrano, Daniel et al. (2019). "Manipulation of focal patterns in acoustic Soret type zone plate lens by using reference radius/phase effect". In: *Ultrasonics* 91, pp. 237–241. ISSN: 0041624X. DOI: `10.1016/j.ultras.2018.07.022` (cit. on pp. 29, 55, 63).

Tu, You-Lin, Shih-Jui Chen, and Yean-Ren Hwang (2016). "Design of Fresnel Lens-Type Multi-Trapping Acoustic Tweezers". In: *Sensors* 16.11, p. 1973. ISSN: 1424-8220. DOI: `10.3390/s16111973` (cit. on pp. 14, 15, 26).

Uchida, Toyoaki et al. (2006). "Treatment of localized prostate cancer using high-intensity focused ultrasound". In: *BJU International* 97.1, pp. 56–61. ISSN: 1464-4096. DOI: `10.1111/j.1464-410X.2006.05864.x` (cit. on p. 64).

Vanderbei, Robert J, David N Spergel, and N Jeremy Kasdin (2003). "Spiderweb masks for high-contrast imaging". In: *The Astrophysical Journal* 590.1, p. 593. ISSN: 0004-637X (cit. on p. 21).

Vilkhu, Kamaljit et al. (2008). "Applications and opportunities for ultrasound assisted extraction in the food industry - A review". In: *Innovative Food*

Science and Emerging Technologies 9.2, pp. 161–169. ISSN: 14668564. DOI: `10.1016/j.ifset.2007.04.014` (cit. on pp. 14, 26).

Wang, Wenqi et al. (2014). "Design and demonstration of broadband thin planar diffractive acoustic lenses". In: *Applied Physics Letters* 105.10, p. 101904. ISSN: 0003-6951. DOI: `10.1063/1.4895619` (cit. on p. 62).

Webb, G. W., I. V. Minin, and O. V. Minin (2007). "New Technique to Suppress Sidelobe Clutter in Perimeter Security Systems". In: *International Journal of High Speed Electronics and Systems* 17.02, pp. 367–382. ISSN: 0129-1564. DOI: `10.1142/S0129156407004564` (cit. on pp. 15, 29).

Welter, John T. et al. (2011). "Focusing of longitudinal ultrasonic waves in air with an aperiodic flat lens". In: *The Journal of the Acoustical Society of America* 130.5, pp. 2789–2796. ISSN: 0001-4966. DOI: `10.1121/1.3640841` (cit. on pp. 14, 26, 50, 63).

Welter, John T. et al. (2012). "Broadband aperiodic air coupled ultrasonic lens". In: *Applied Physics Letters* 100.21, p. 214102. ISSN: 0003-6951. DOI: `10.1063/1.4720149` (cit. on p. 63).

Wenzel, Richard P (1995). "Nosocomial candidemia: risk factors and attributable mortality". In: *Clinical Infectious Diseases* 20.6, pp. 1531–1534 (cit. on p. 4).

WHO, World Health Organization (2020a). "Cancer Mortality Database". In: *Online repository accessed August 2020:* `http://www-dep.iarc.fr/WHOdb/WHOdb.htm.` (cit. on p. 1).

— (2020b). "Global Cancer Observatory". In: *Online repository accessed August 2020:* `https://gco.iarc.fr` (cit. on p. 1).

Wood, R. W. (1898). "LIII. Phase-reversal zone-plates, and diffraction-telescopes". In: *The London, Edinburgh, and Dublin Philosophical Magazine and Journal of Science* 45.277, pp. 511–522. ISSN: 1941-5982. DOI: `10.1080/14786449808621159` (cit. on p. 40).

Xia, Xiangxiang et al. (2018). "Planar Ultrasonic Lenses Formed by Concentric Circular Sandwiched-Ring Arrays". In: *Advanced Materials Technologies,*

p. 1800542. ISSN: 2365-709X. DOI: `10.1002/admt.201800542` (cit. on p. 62).

Xu, Zheng et al. (2017). "A flat acoustic lens to generate a Bessel-like beam". In: *Ultrasonics* 80, pp. 66–71. ISSN: 0041624X. DOI: `10.1016/j.ultras.2017.05.005` (cit. on pp. 28, 41).

Yamada, Ken and Hiroshi Shimizu (1982). "New Types of Ultrasound Focusing Transducer Sysmtems". In: *Japanese Journal of Applied Physics* 21.S3, p. 135. ISSN: 0021-4922. DOI: `10.7567/JJAPS.21S3.135` (cit. on p. 40).

— (1991). "Planar-structure focusing lens for acoustic microscope." In: *Journal of the Acoustical Society of Japan (E)* 12.3, pp. 123–129. ISSN: 0388-2861. DOI: `10.1250/ast.12.123` (cit. on p. 40).

Yang, Xishan et al. (2015). "Acoustic superlens using Helmholtz-resonator-based metamaterials". In: *Applied Physics Letters* 107.19, p. 193505. ISSN: 0003-6951. DOI: `10.1063/1.4935589` (cit. on p. 62).

Zhang, Shu, Leilei Yin, and Nicholas Fang (2009). "Focusing Ultrasound with an Acoustic Metamaterial Network". In: *Physical Review Letters* 102.19, p. 194301. ISSN: 0031-9007. DOI: `10.1103/PhysRevLett.102.194301` (cit. on pp. 14, 27).

Zhu, Jie et al. (2011). "A holey-structured metamaterial for acoustic deep-subwavelength imaging". In: *Nature physics* 7.1, pp. 52–55 (cit. on p. 4).

Zhu, Xu and Eun Sok Kim (1998). "Microfluidic motion generation with acoustic waves". In: *Sensors and Actuators A: Physical* 66.1-3, pp. 355–360. ISSN: 09244247. DOI: `10.1016/S0924-4247(97)01712-3` (cit. on p. 40).

Zienkiewicz, Olgierd Cecil et al. (1977). *The finite element method.* Vol. 3. McGraw-hill London (cit. on pp. 15, 54).